Image-based surface reconstruction in geomorphometry – merits, limits and developments

A. Eltner[1], A. Kaiser[2], C. Castillo[3], G. Rock[4], F. Neugirg[5] and A. Abellan[6]

[1] {Institute of Photogrammetry and Remote Sensing, Technical University Dresden, Germany}

[2] {Soil and Water Conservation Unit, Technical University Freiberg, Germany}

[3] {Dep. of Rural Engineering, University of Córdoba, Spain}

[4] {Dep. of Environmental Remote Sensing and Geomatics, University of Trier, Germany}

[5] {Dep. of Physical Geography, Catholic University Eichstätt-Ingolstadt, Germany}

[6] {Risk Analysis Group, Institute of Earth Sciences, University of Lausanne, Switzerland}

Correspondence to: A. Eltner (Anette.Eltner@tu-dresden.de)

Abstract

Photogrammetry and geosciences have been closely linked since the late 19th century due to the acquisition of high-quality 3D datasets of the environment, but it has so far been restricted to a limited range of remote sensing specialists because of the considerable cost of metric systems for the acquisition and treatment of airborne imagery; Nowadays, a wide range of commercial and open-source software tools enable the generation of 3D and 4D models of complex geomorphological features by geoscientists and other non-experts users. In addition, very recent rapid developments in unmanned aerial vehicle (UAV) technology allows for the flexible generation of high quality aerial surveying and orthophotography at a relatively low-cost.

The increasing computing capabilities during the last decade, together with the development of high-performance digital sensors and the important software innovations developed by computer based vision and visual perception research fields has extended the rigorous processing of stereoscopic image data to a 3D point cloud generation from a series of non-calibrated images. Structure from motion (SfM) workflows are based upon algorithms for efficient and automatic orientation of large image sets without further data acquisition information, examples including robust feature detectors like the scale-invariant feature

transform for 2D-imagery. Nevertheless, the importance of carrying out well-established fieldwork strategies, using proper camera settings, ground control points and ground truth for understanding the different sources of errors still need to be adapted in the common scientific practice.

This review intends not only to summarize the current state of the art on using SfM workflows in geomorphometry, but also to give an overview of terms and fields of application. Further this article aims to quantify already achieved accuracies and used scales using different strategies, to evaluate possible stagnations of current developments and to identify key future challenges. It is our belief that some lessons learned in already published articles, scientific reports and book chapters concerning the identification of common errors or "bad practices" and some other valuable information may help in guiding the future use of SfM photogrammetry in geosciences.

1 Introduction

Early works on projective geometries date back to more than five centuries, when scientists derived coordinates of points from several images and investigated the geometry of perspectives. Projective geometry represents the basis for the developments in photogrammetry in the late 19th century, when Aimé Laussedat experimented with terrestrial imagery as well as kites and balloons for obtaining imagery for topographic mapping (Laussedat, 1899). Rapidly, photogrammetry advanced to be an essential tool in geosciences during the last two decades and is lately gaining momentum driven by digital sensors. Simultaneously, growing computing capacities and rapid developments in computer vision led to the method of Structure from Motion (SfM) that opened the way for low-cost high-resolution topography. Thus, the community using image-based 3D reconstruction experienced a considerable growth, not only in quality and detail of the achieved results but also in the number of potential users from diverse geo-scientific disciplines.

SfM photogrammetry can be performed with images acquired with consumer grade digital cameras and is thus very flexible in its implementation. Its ease of use in regard to data acquisition and processing makes it further interesting to non-experts (Fig. 1). The diversity of possible applications led to a variety of terms used to describe SfM photogrammetry either from photogrammetric or computer vision standpoint. Thus to avoid ambiguous terminology, a short list of definitions in regard to the reviewed method is given in Table 1. In this review a series of studies that utilise the algorithmic advance of high automatisation in SfM are

considered, i.e. no initial estimates of the image network geometry or user interactions to generate initial estimates are needed. Furthermore, data processing can be performed almost fully automatic. However, some parameter settings, typical for photogrammetric tools (e.g. camera calibration values), can be applied to optimise both accuracy and precision, and GCP or scale identification are still necessary.

SfM photogrammetry can be applied to a vast range of temporal as well as spatial scales and resolutions up to an unprecedented level of detail, allowing for new insights into earth surface processes, i.e. 4D (three spatial dimensions and one temporal dimension) reconstruction of environmental dynamics. For instance, the concept of sediment connectivity (Bracken et al., 2014) can be approached from a new perspective through varying spatio-temporal scales. Thereby, the magnitude and frequency of events and their interaction can also be evaluated. Furthermore, the versatility of SfM photogrammetry utilising images captured from aerial or terrestrial perspectives has the advantage of being applicable in remote areas with limited access and in fragile, fast changing environments.

After the suitability of SfM has been noticed for geo-scientific applications (James and Robson, 2012, Westoby et al., 2012, Fonstad et al., 2013) the number of studies utilising SfM photogrammetry for geomorphometric investigations (thereby referring to the "science of topographic quantification" after Pike et al., 2008) has increased significantly. However, the method needs sophisticated study design and some experience in image acquisition to prevent predictable errors and to ensure good quality of the reconstructed scene.Smith et al. (2015) and Micheletti et al. (2015) recommend a setup for efficient data acquisition.

A total of 65 publications are reviewed in this study. They are chosen according to the respective field of research and methodology. Only studies are included that make use of the benefits of automatic image matching algorithms and thus apply the various SfM tools. Studies that lack of full automatisation are excluded, i.e. some traditional photogrammetric software. Topic wise a line is drawn in regard to the term geosciences. The largest fraction of the reviewed articles tackles questions arising in geomorphological contexts. To account for the versatility of SfM photogrammetry, a few studies deal with plant growth on different scales (moss, crops, forest) or investigate rather exotic topics such as stalagmites or reef morphology.

This review aims to highlight the development of SfM photogrammetry as a great tool for geoscientists:

(1) The method of SfM photogrammetry is briefly summarised and algorithmic differences due to their emergence from computer vision as well as photogrammetry are clarified (section 2).
(2) Open-source tools regarding SfM photogrammetry are introduced as well as beneficial tools for data post-processing (section 3).
(3) Different fields of applications where SfM photogrammetry led to new perceptions in geomorphometry are displayed (section 4).
(4) The performance of the reviewed method is evaluated (section 5).
(5) And frontiers and significance of SfM photogrammetry are discussed (section 6).

2 SfM photogrammetry: method outline

2.1 Basic concept

Reconstruction of three-dimensional geometries from images has played an important role in the past centuries (Ducher, 1987, Collier, 2002). The production of high-resolution DEMs was and still is one of the main applications of (digital) photogrammetry. Software and hardware developments as well as the increase in computing power in the 1990s and early 2000s made aerial photogrammetric processing of large image datasets accessible to a wider community (e.g. Chandler, 1999).

Camera orientations and positions, which are usually unknown during image acquisition, have to be reconstructed to model a 3D scene. For that purpose, photogrammetry has developed bundle adjustment (BA) techniques, which allowed for simultaneous determination of camera orientation and position parameters as well as 3D object point coordinates for a large number of images (e.g. Triggs et al, 2000). The input into the BA are image coordinates of many tie points. If the BA is extended by a simultaneous calibration option, even the intrinsic camera parameters can be determined in addition to the extrinsic parameters. Furthermore, a series of ground control points can be used as input into BA for geo-referencing the image block (e.g. Luhmann et al., 2014, Kraus, 2007, Mikhail et al., 2001).

Parallel developments in computer vision took place that try to reconstruct viewing geometries of image datasets not fulfilling the common prerequisites from digital photogrammetry, i.e. calibrated cameras and initial estimates of the image acquisition scheme. This led to the SfM technique (Ullman, 1979) allowing to process large datasets and to use a combination of multiple non-metric cameras.

The typical workflow of SfM photogrammetry (e.g. Snavely et al., 2008) comprises the following steps:

(1) identification and matching of homologous image points in overlapping photos (image matching),
(2) reconstruction of the geometric image acquisition configuration and of the corresponding 3D coordinates of matched image points (sparse point cloud) with iterative BA,
(3) dense matching of the sparse point cloud from reconstructed image network geometry,
(4) scaling or geo-referencing, which is also performable within step 2.

Smith et al. (2015) give a detailed description of the workflow of SfM photogrammetry, especially regarding step 1 and step 2.

In contrast to classical photogrammetry software tools, SfM allows for reliable processing of a large number of images in rather irregular image acquisition schemes (Snavely et al., 2008) with a much higher degree of process automation. Thus, one of the main differences between usual photogrammetric workflow and SfM is the emphasis on either accuracy or automation, with SfM focusing on the latter (Pierrot-Deseilligny and Clery, 2011). Another deviation between both 3D reconstruction methods is the consideration of GCPs (James and Robson, 2014, Eltner and Schneider, 2015). Photogrammetry performs BA either one-staged, considering GCPs within the BA, or two-staged, performing geo-referencing after a relative image network configuration has been estimated (Kraus, 2007). In contrast, SfM is solely performed in the manner of a two-staged BA concentrating on the relative orientation in an arbitrary coordinate system. Thus, absolute orientation has to be conducted separately with a seven parameter 3D-Helmerttransformation, i.e. three shifts, three rotations and one scale. This can be done, for instance, with the freeware tool sfm-georef that also gives accuracy information (James and Robson, 2012). Using GCPs has been proven to be relevant for specific geometric image network configurations, as parallel-axes image orientations usual for UAV data, because adverse error propagation can occur due to unfavourable parameter correlation, e.g. resulting in the non-linear error of a DEM dome (Wu, 2014, James and Robson, 2014, Eltner and Schneider, 2015). Within a one-staged BA these errors are minimised because during the adjustment calculation additional information from GCPs is employed, which is not possible, when relative and absolute orientation are not conducted in one stage.

The resulting oriented image block allows for a subsequent dense matching, measuring many more surface points through spatial intersection to generate a DEM with very high resolution.

Recent developments in dense matching allow for resolving object coordinates for almost every pixel. To estimate 3D coordinates, pixel values are either compared in image-space in the case of stereo-matching, considering two images, or in the object space in the case of MVS-matching, considering more than two images (Remondino et al., 2014). Furthermore, local or global optimisation functions (Brown et al., 2003) are considered, e.g. to handle ambiguities and occlusion effects between compared pixels (e.g. Pears et al., 2012). To optimise pixel matching, (semi-)global constraints consider the entire image or image scan-lines (e.g. semi-global matching (SGM) after Hirschmüller, 2011), whereas local constraints consider a small area in direct vicinity of the pixel of interest (Remondino et al., 2014).

SfM photogrammetry software packages are available partially as freeware or even open-source. Most of the packages comprise SfM techniques in order to derive 3D reconstructions from any collection of unordered photographs, without the need of providing camera calibration parameters and high accuracy ground control points. As a consequence, no in-depth knowledge in photogrammetric image processing is required in order to reconstruct geometries from overlapping image collections (James and Robson, 2012, Westoby et al., 2012, Fonstad et al., 2013). But now, also many photogrammetric tools utilise abilities from SfM to derive initial estimates automatically (i.e. automation) and then perform photogrammetric BA with the possibility to set weights of parameters for accurate reconstruction performance (i.e. accuracy). In this review studies are considered, which either use straight SfM tools from computer vision or photogrammetric tools implementing SfM algorithms that entail no need for initial estimates in any regard.

2.2 Tools for SfM photogrammetry and data post processing

SfM methodologies rely inherently on automated processing tools which can be provided by different non-commercial or commercial software packages. Within the commercial approach PhotoScan (Agisoft LLC, Russia), Pix4D (Pix4D SA, Switzerland) and MENCI APS (MENCI Software, Italy) represent complete solutions for 3D photogrammetric processing that have been used in several of the reviewed works.

Initiatives based on non-commercial software have played a significant role in the development of SfM photogrammetry approaches, either 1) open-source, meaning the source code is available with a license for modification and distribution; 2) freely-available, meaning the tool is free to use but no source code is provided or 3) under free web service with no access to the code, intermediate results or possible secondary data usage (Table 2). The

194 pioneer works by Snavely et al. (2006, 2008) and Furukawa and Ponce (2010) as well as
195 Furukawa et al. (2010) provided the basis to implement one of the first open-source
196 workflows for free SfM photogrammetry combining Bundler and PMVS2/CMVS as in
197 SfMToolkit (Astre, 2015). By 2007, the MicMac project, which is open-source software
198 originally developed for aerial image matching, became available to the public and later
199 evolved to a comprehensive SfM photogrammetry pipeline with further tools such as APERO
200 (Pierrot-Deseilligny and Clery, 2011).

201 Further contributors put their efforts in offering freely-available solutions based on Graphical
202 User Interfaces (GUI) for SfM photogrammetry (VisualSfM by Wu, 2013) and geo-
203 referencing (sfm_georef by James and Robson, 2012). The need for editing large point-cloud
204 entities from 3D reconstruction led to the development of open-source specific tools such as
205 Meshlab (Cignoni et al., 2008) or CloudCompare (Girardeau-Montaut, 2015), also
206 implementing GUIs. Sf3M (Castillo et al., 2015) exploits VisualSfM and sfm_georef and
207 additional CloudCompare command-line capacities for image-based surface reconstruction
208 and subsequent point cloud editing within one GUI tool. Overall, non-commercial
209 applications have provided a wide range of SfM photogrammetry related solutions that are
210 constantly being improved on the basis of collaborative efforts. Commercial software
211 packages are not further displayed due to their usual lack of detailed information regarding
212 applied algorithms and their black box approach.

213 A variety of tools of SfM photogrammetry (at least 10 different) are used within the differing
214 studies of this review (Fig. 3). Agisoft PhotoScan is by far the most employed software,
215 which is probably due to its ease of use. However, this software is commercial and works
216 after the black box principle, which is in contrast to the second most popular tools Bundler in
217 combination with PMVS or CMVS. The tool APERO in combination with MicMac focuses
218 on accuracy instead of automation (Pierrot-Deseilligny and Clery, 2011), which is different to
219 the former two. The high degree of possible user-software interaction that can be very
220 advantageous to adopt the 3D reconstruction to each specific case study might also be its
221 drawback because further knowledge into the method is required. Only a few studies have
222 used the software in geo-scientific investigations (Bretar, et al., 2013, Stumpf et al., 2014,
223 Ouédraogo et al., 2014, Stöcker et al., 2015, Eltner and Schneider, 2015).

224

3 Approaches to identify key developments of SfM photogrammetry

The vast recognition of SfM photogrammetry resulted in a large variety of its implementation leading to methodological developments, which have validity beyond its original application. Thus regarding geomorphometric investigations, studies considering field of applications as well as evaluations of the method performance induced key advances for SfM photogrammetry to establish as a standard tool in geosciences (Table 3). In the following, the approaches are introduced concerning the selection and retrieval of scientific papers utilising SfM photogrammetry and methods illustrated concerning integrated consideration of error performance of SfM photogrammetry in geo-scientific studies.

3.1 Selection of scientific papers exploiting SfM photogrammetry

A survey of 65 scientific papers published between 2012 and 2015 was conducted, covering a wide range of applications of SfM photogrammetry in geo-scientific analysis (see Appendix A for a detailed list). Common scientific journals, academic databases and standard online searches have been used to search for corresponding publications. Although, it has to be noted that our approach does not guarantee full coverage of the published works using SfM photogrammetry in geosciences. Nevertheless, various disciplines, locations and approaches from all continents are contained in this review (Fig. 2).

To put research hot spots in perspective it should be taken into account that the amount of publications in each discipline is not only dependent on the applicability of the method in that specific field of research. To a greater degree it is closely linked to the overall number of studies, which in the end can probably be broken down to the actual amount of researchers in that branch of science. Relative figures revealing the relation between SfM photogrammetry oriented studies to all studies of a given field of research would be desirable but are beyond the scope of this review.

3.2 Performing error evaluation from recent studies

SfM photogrammetry has been tested under a large variety of environments due to the commensurate novel establishment of the method in geosciences, revealing numerous advantages but also disadvantages regarding to each application. It is important to have method independent references to evaluate 3D reconstruction tools confidently. In total 39 studies are investigated (Table Appendix A), where a reference has been setup, either area

based (e.g. TLS) or point based (e.g. RTK GPS points). Because not all studies perform accuracy assessment with independent references, the number of studies is in contrast to the number of 65 studies that are reviewed in regard to applications.

A designation of error parameters is performed prior to comparing the studies to avoid using ambiguous terms. There is a difference between local surface quality and more systematic errors, i.e. due to referencing and project geometry (James and Robson, 2012). Specifically, error can be assessed in regard to accuracy and precision.

Measurement accuracy, which defines the closeness of the measurement to a reference ideally displays the true surface and can be estimated by the mean error value. However, positive and negative deviations can compensate for each other and thus can impede the recognition of a systematic error (e.g. symmetric tilting) with the mean value. Therefore, numerical and spatial error distribution should also be considered to investigate the quality of the measurement (e.g. Smith et al., 2015). For the evaluation of two DEMs, the iterative closest point (ICP) algorithm can improve the accuracy significantly if a systematic linear error (e.g. shifts, tilts or scale variations) is given, as demonstrated by Micheletti et al. (2014); Nevertheless, this procedure can also induce an error when the scene has changed significantly between the two datasets.

Precision, which defines the repeatability of the measurement, e.g. it indicates how rough an actual planar surface is represented, usually comprises random errors that can be measured with the standard deviation or RMSE. However, precision is not independent from systematic errors. In this study, the focus lies on RMSE or standard deviation calculated to a given reference (e.g. to a LiDAR - light detection and ranging - point cloud) and thus the general term “measured error” is used.

Furthermore, error ratios are calculated to compare SfM photogrammetry performance between different studies under varying data acquisition and processing conditions. Thereby, the relative error (e_r), the reference superiority (e_s) and the theoretical error ratio (e_t) are considered. The first is defined as the ratio between measured error and surface to camera distance (eq. 1).

$$e_r = \frac{\sigma_m}{D} \tag{1}$$

Being:

$e_r \dots relative\ error$

$\sigma_m \dots measured\ error$

$D \ldots mean\ distance\ camera - surface$

The reference superiority displays the ratio between the measured error and the error of the reference (eq. 2). It depicts the validity of the reference to be accountable as a reliable dataset for comparison.

$$e_s = \frac{\sigma_m}{\sigma_{ref}} \quad (2)$$

Being:

$e_r \ldots reference\ superiority$

$\sigma_{ref} \ldots reference\ error$

The theoretical error ratio includes the theoretical error, which is an estimate of the theoretically best achievable photogrammetric performance under ideal conditions. It is calculated separately for convergent and parallel-axes image acquisition schemes. The estimate of the theoretical error of depth measurement for the parallel-axis case is displayed by eq. 3 (more detail in Kraus, 2007). The error is determined for a stereo-image pair and thus might overestimate the error for multi-view reconstruction. Basically, the error is influenced by the focal length, the camera to surface distance and the distance between the images of the stereo-pair (base).

$$\sigma_p = \frac{D^2}{Bc}\sigma_i \quad (3)$$

Being:

$\sigma_p \ldots coordinate\ error\ for\ parallel - axes\ case$

$c \ldots focal\ length$

$\sigma_i \ldots error\ image\ measurement$

$B \ldots distance\ between\ images\ (base)$

For the convergent case the error also considers the camera to surface distance and the focal length. However, instead of the base the strength of image configuration determined by the angle between intersecting homologous rays is integrated and additionally the employed number of images is accounted for (eq. 4; more detail in Luhmann et al., 2014).

$$\sigma_c = \frac{qD}{\sqrt{k}c}\sigma_i \quad (4)$$

311 Being:

σ_c … $coordinate\ error\ for\ convergent\ case$

q … $strength\ of\ image\ configuration, i.e. convergence$

k … $number\ of\ images$

312

313 Finally, the theoretical error ratio is calculated displaying the relation between the measured
314 error and the theoretical error (eq. 5). The value depicts the performance of SfM
315 photogrammetry in regard to the expected accuracy.

316 $$e_t = \frac{\sigma_m}{\sigma_{theo}} \quad (5)$$

317 Being:

318 e_t … $theoretical\ error\ ratio$

σ_{theo} … $theoretical\ error;\ eihter\ \sigma_p\ or\ \sigma_c$

319

320 The statistical analysis of the achieved precisions of the reviewed studies is performed with
321 the Python Data Analysis Library (pandas). If several errors are given in one study due testing
322 of different survey or processing conditions, the error value representing the enhancement of
323 the SfM performance has been chosen, i.e. in the study of Javernick et al. (2014) the DEM
324 without an error dome, of Rippin et al. (2015) the linear corrected DEM, and of Eltner &
325 Schneider (2015) the DEMs calculated with undistorted images. In addition, if several
326 approaches are conducted to retrieve the deviations value to the reference, the more reliable
327 error measure is preferred (regards Stumpf et al., 2014 and Gómez-Gutiérrez et al., 2014 and
328 2015). Apart from those considerations, measured errors have been averaged if several values
329 are reported in one study, i.e. concerning multi-temporal assessments or consideration of
330 multiple surfaces with similar characteristics, but not for the case of different tested SfM
331 tools. Regarding data visualisation, outliers that complicated plot drawing, were neglected
332 within the concerning graphics. This concerned the study of Dietrich (2016) due to a very
333 large scale of an investigated river reach (excluded from Fig. 4a and Fig. 5a-b), the study of
334 Snapir et al. (2014) due to a very high reference accuracy of Lego bricks (excluded from Fig.
335 4c and Fig. 5b), and Frankl et al. (2015) due to a high measured error as the study focus was
336 rather on feasibility than accuracy (excluded from Fig. 5c).

337 Besides exploiting a reference to estimate the performance of the 3D reconstruction,
338 registration residuals of GCPs resulting from BA can be taken into account for a first error
339 assessment. But it is not suitable as exclusive error measure due to potential deviations

between the true surface and the calculated statistical and geometric model, which are not detectable with the GCP error vectors alone because BA is optimised to minimise the error at these positions. However, if BA has been performed two-staged (i.e. SfM and referencing calculated separately), the residual vector provides reliable quality information because registration points are not integrated into model estimation.

4 Recent applications of SfM photogrammetry in geosciences

The previously described advantages of the method has introduced a new group of users, leading to a variety of new studies in geomorphic surface reconstruction and analysis. Different disciplines started to use SfM algorithms more or less simultaneously.

A list of all topics reviewed in this manuscript according to their year of appearance is shown in Table 4. It is important to note that most subjects are not strictly separable from each other: For instance, a heavy flash flood event will likely trigger heavy damage by soil erosion or upstream slope failures. Thus, corresponding studies are arranged in regard to their major focus. The topic soil science comprises studies of soil erosion as well as soil micro-topography.

4.1 Soil science

An identification of convergent research topics of SfM photogrammetry in geosciences revealed a distinct focus on erosional processes, especially in soil erosion (11 studies). Gullies, as often unvegetated and morphologically complex features of soil erosion, are predestined to serve as a research object (6 studies) to evaluate SfM performance. One of the first works on SfM in geosciences from 2012 compared established 2D and 3D field methods for assessing gully erosion (e.g. LiDAR, profile meter, total station) to SfM datawith regard to costs, accuracy and effectiveness revealing the superiority of the method (Castillo et al., 2012). Also for a gully system, Stöcker et al. (2015) demonstrated the flexibility of camera based surface reconstructionby combining independently captured terrestrial images with surface models from UAV images to fill data gaps and achieve a comprehensive 3D model. Large areal coverage and very high resolution - allowed for a new quality in the assessment of plot based soil erosion analysis (Eltner et al., 2015)

Another 6 studies tackle the 3D reconstruction of soil micro-topography by producing very dense point clouds or DEMs. This data further serves to assess pros and cons of SfM

372 photogrammetry, e.g. to detect small-scale erosion features (Nouwakpo et al., 2014), with
373 regard to the doming effect (Eltner and Schneider, 2015) or as input parameter for erosion
374 modelling (Kaiser et al., 2015).

375

376 ## 4.2 Volcanology

377 Volcanology is a pioneering area of SfM photogrammetry research in geosciences because 3
378 out of 6 studies in 2012 included volcanic research sites. James and Robson (2012) acquired
379 information on volcanic dome volume and structural variability prior to an explosion from
380 multi-temporal imagery taken from a light airplane. Another interesting work by Bretar et al.
381 (2013) successfully reveals roughness differences in volcanic surfaces from lapilli deposits to
382 slabby pahoehoe lava.

383

384 ## 4.3 Glaciology

385 Glaciology and associated moraines are examined in 7 publications. In several UAV
386 campaigns Immerzeel et al. (2014) detected limited mass losses and low surface velocities but
387 high local variations of melt rates that are linked to supra-glacial ponds and ice cliffs. Rippin
388 et al. (2015) present another UAV-based work on supra-glacial runoff networks, comparing
389 the drainage system to surface roughness and surface reflectance measurements and detecting
390 linkages between all three. Furthermore, snow depth estimation and rock glacier monitoring
391 are increasingly performed with SfM photogrammetry (Nolan et al., 2015, Dall'Asta et al.,
392 2015).

393

394 ## 4.4 Mass movements

395 Compared to the well-stablished use of LiDAR techniques on the investigation of landslides
396 (Jaboyedoff et al., 2012) the use of photogrammetric workflows for investigating hazardous
397 slopes is still scarce, wich is probably due to the stringent accuracy and safety
398 requirements.For instance, the use of UAV systems for monitoring mass movements using
399 both image correlation algorithms and DM substraction techniques has been explored by
400 Lucieer et al., (2013). More recently, SfM techniques were used by Stumpf et al. (2014) for
401 monitoring landslide displacements and erosion during several measuring campaigns,
402 including the study of seasonal dynamics on the landslide body, superficial deformation and

rock fall occurrence. In addition, thes authors assessed the accuracy of two different 3D reconstruction tools compared to LiDAR data.

4.5 Fluvial morphology

Channel networks in floodplains were surveyed by Prosdocimi et al. (2015) in order to analyse eroded channel banks and to quantify the transported material. Besides classic DSLR cameras, evaluation of an iPhone camera revealed sufficient accuracy, so that in near future also non-scientist are able to carry out post event documentation of damage. An interesting large scale riverscape assessment is presented by Dietrich (2016), who carried out a helicopter based data acquisition of a 32 km river segment. A small helicopter proves to close the gap between unmanned platforms and commercial aerial photography from airplanes.

4.6 Coastal morphology

In the article by Westoby et al. (2012) several morphological features of contrasting landscapes where chosen to test the capabilities of SfM; one of them being a coastal cliff of roughly 80 m height. Up to 90.000 points/m² enabled the identification of bedrock faulting. Ružić et al. (2014) produced surface models of coastal cliffs to test the abilities of SfM photogrammetry in undercuts and complex morphologies.

4.7 Other fields of investigation in geosciences

In addition to the prevalent fields of attention also more exotic research is carried out unveiling unexpected possibilities for SfM photogrammetry. Besides the benefit for the specific research itself, these branches are important as they either explore new frontiers in geomorphometry or demonstrate the versatility of the method. Lucieer et al. (2014) analyse artic moss beds and their health conditions by using high-resolution surface topography (2 cm DEM) to simulate water availability from snow melt. Leon et al. (2015) acquired underwater imagery of a coral reef to produce a DEM with a resolution of 1 mm for roughness estimation. Genchi et al. (2015) used UAV-image data of an urban cliff structure to identify bio erosion features and found a pattern in preferential locations.

The re-consideration of historical aerial images is another interesting opportunity arising from the new algorithmic image matching developments that allow for new DEM resolutions and thus possible new insights into landscape evolution (Gomez et al., 2015).

5 Error assessment of SfM photogrammetry in geo-scientific applications

Error evaluation in this study is performed with reference measurements. Thereby, errors due the performance of the method itself and errors due to the method of quality assessment have to be distinguished.

5.1 Error sources of SfM photogrammetry

The error of 3D reconstruction is influenced by many factors: scale/distance, camera calibration, image network geometry, image matching performance, surface texture and lighting conditions, and GCP characteristics, which are examined in detail in this section.

Scale and sensor to surface distance

SfM photogrammetry contains the advantage to be useable at almost any scale. Thus, in the reviewed studies the method is applied at a large range of scales (Fig. 4a), reaching from 10 cm for volcanic bombs (Favalli et al., 2012, James and Robson, 2012) up to 10 km for a river reach (Dietrich, 2016). Median scale amounts about 100 m. SfM photogrammetry reveals a scale dependent practicability (Smith and Vericat, 2015) if case study specific tolerable errors are considered, e.g. for multi-temporal assessments. For instance, at plot and hillslope scale 3D reconstruction is a very sufficient method for soil erosion studies, even outperforming TLS (Nouwakpo et al., 2015, Eltner et al., 2015, Smith and Vericat, 2015). The method should be most useful in small scale study reaches (Fonstad et al., 2013), whereas error behaviour is not as advantageous for larger scales, i.e. catchments (Smith and Vericat, 2015).

Besides scale, the distance between sensor and surface is important for image-based reconstructed DEM error, also because scale and distance interrelate. The comparison of the reviewed studies indicates that with an increase of distance the measured error increases, which is not unexpected (Fig. 5a, circles). However, there is no linear trend detectable.

463 Therefore, the relative error is not assignable. The relative error displays a large range from
464 15 to 4000 with a median of 400, thus revealing a rather low error potential (Fig. 5a,
465 triangles). Very high ratios are solely observable for very close-range applications and at large
466 distances. A general increase of the relative error with distance is observable (Fig. 5a,
467 triangles). The indication that cm-accurate measurements are realisable at distances below
468 200 m (Stumpf et al., 2014) can be confirmed by Fig. 5a because most deviations are below
469 10 cm until that range. Overall, absolute error values are low at close ranges, whereas the
470 relative error is higher at larger distances.

471

472 *Camera calibration*

473 SfM photogrammetry allows for straight forward handling of camera options due to integrated
474 self-calibration, but knowledge about some basic parameters is necessary to avoid unwanted
475 error propagation into the final DEM from insufficiently estimated camera models. The
476 autofocus as well as automatic camera stabilisation options should be deactivated if a pre-
477 calibrated camera model is used or one camera model is estimated for the entire image block
478 because changes in the interior camera geometry due to camera movement cannot be captured
479 with these settings. The estimation of a single camera model for one image block is usually
480 preferable, if a single camera has been used, whose interior geometry is temporary stable, to
481 avoid over parameterisation (Pierrot-Deseilligny and Clery, 2011). Thus, if zoom lenses are
482 moved a lot during data acquisition, they should be avoided due to their instable geometry
483 (Shortis et al., 2006, Sanz-Ablanedo et al., 2010) that impedes usage of pre-calibrated fixed or
484 single camera models. A good compromise between camera stability, sensor size and
485 equipment weight, which is more relevant for UAV applications, are achieved by compact
486 system cameras (Eltner and Schneider, 2015). However, solely three studies utilize compact
487 system cameras in the reviewed studies (Tonkin et al., 2014, Eltner and Schneider, 2015,
488 Eltner et al., 2015).

489 Along with camera settings, the complexity in regard to the considered parameters of the
490 defined camera model within the 3D reconstruction tool is relevant as well as the
491 implementation of GCPs to function as further observation in the BA, i.e. to avoid DEM
492 domes as a consequence of insufficient image distortion estimation (James and Robson, 2014,
493 Eltner and Schneider, 2015). Also, Stumpf et al. (2014) detect worse distortion correction
494 with a basic SfM tool, considering a simple camera model, compared to more complex
495 software, integrating a variety of camera models and GCP consideration. Camera calibration

is a key element for high DEM quality, which is extensively considered in photogrammetric software, whereas simpler models that solely estimate principle distance and radial distortion are usually implemented in the SfM tools originating from computer vision (Eltner and Schneider, 2015, James and Robson, 2012, Pierrot-Deseilligny and Clery, 2011).

Image resolution

Image resolution is another factor influencing the final DEM quality. Especially, the absolute pixel size needs to be accounted for due to its relevance for the signal-to-noise ratio (SNR) because the larger the pixel the higher the amount of light that can be captured and hence a more distinct signal is measured. Resolution alone by means of pixel number gives no information about the actual metric sensor size. A large sensor with large pixels and a large amount of pixels provides better image quality due to reduced image noise than a small sensor with small pixels but the same amount of pixels. Thus, high image resolution defined by large pixel numbers and pixel sizes resolves in sufficient quality of images and thus DEMs (Micheletti et al., 2014, Eltner and Schneider, 2015).

However, the reviewed investigations indicate no obvious influence of the pixel size at the DEM quality. Mostly, cameras with middle sized sensors and corresponding pixel sizes around 5 µm are used and a large range of error at different pixel sizes is given.

To speed up processing, down-sampling of images is often performed causing interpolation of pixels and thus the reduction of image information, which can be the cause for underestimation of high relief changes, e.g., observed by Smith and Vericat (2015) or Nouwakpo et al. (2015). Interestingly, Prosdocimi et al. (2015) reveal that lower errors are possible with decreasing resolution due to an increase of error smoothing. Nevertheless, image data collection in the field should be done at highest realisable resolution and highest SNR to fully keep control over subsequent data processing, i.e. data smoothing should be performed under self-determined conditions at the desktop, which is especially important for studies of rough surfaces to allow for probate error statistics (e.g. Brasington et al., 2012).

Image network geometry

In regard to the geometry of the image network several parameters are important: number of images, image overlap, obliqueness and convergence.

At least three images need to capture the area of interest, but for redundancy to decrease DEM error higher numbers are preferred (James and Robson, 2012). For instance, Piermattei et al. (2015) detect better qualities for a higher amount of images. However, the increase of images does not linearly increase the accuracy (Micheletti et al., 2014), and may ultimately lead to unnecessary increase in computation time. Generally, image number should be chosen depending on the size and complexity of the study reach (James and Robson, 2012); as high as possible but still keeping in mind acceptable processing time.

High image overlap is relevant to finding homologous points within many images that cover the entire image space. Stumpf et al. (2014) show that higher overlap resolves in better results. Wide angle lenses, whose radial distortion is within the limits, should be chosen for data acquisition.

The reviewed studies reveal a large variety of applicable perspectives for DEM generation. Most applications use images captured from the ground, which is the most flexible implementation of the SfM photogrammetry method. In regard to terrestrial or aerial perspective, Smith and Vericat (2015) state that aerial images should be preferred if plots reach sizes larger 100 m because at these distances obliqueness of images becomes too adverse. Stumpf et al. (2014) even mention a distinct value of the incidence angle of 30° to the captured surface above which data quality decreases significantly.

Furthermore, image network geometry has to be considered separately for convergent acquisitions schemes, common for terrestrial data collection, and for parallel-axes acquisition schemes, common for aerial data collection. The parallel-axes image configuration results in unfavourable error propagation due to unfavourable parameter correlation, which inherits the separation between DEM shape and radial distortion (James and Robson, 2014, Wu, 2014) resulting in a dome error that needs either GCP implementation or a well estimated camera model for error mitigation (James and Robson, 2014, Eltner and Schneider, 2015). However, GCP accuracy has to be sufficient or else the weight of GCP information during BA is too low to avoid unfavourable correlations, as shown by Dietrich (2016), where DEM dome error within a river reach could not be diminished even though GCPs were implemented into 3D reconstruction. If convergent images are utilised, the angle of convergence is important because the higher the angle the better the image network geometry. Thereby, accuracy increases because sufficient image overlap is possible with larger bases between images. Therefore, glancing ray intersections, which impede distinct depth assignment, are avoided. But simultaneously, convergence should not be so high that the imaged scene becomes too

560 contradictory for successful image matching (Pierrot-Deseilligny and Clery, 2012, Stöcker et
561 al, 2015).

562

563 *Accuracy and distribution of homologues image points*

564 The quality of DEMs reconstructed from overlapping images depends significantly on the
565 image-matching performance (Grün, 2012). Image content and type, which cannot be
566 enhanced substantially, are the primary factors controlling the success of image-matching
567 (Grün, 2012). Image-matching is important for reconstruction of the image network geometry
568 as well as the subsequent dense-matching.

569 On the one hand, it is relevant to find good initial matches (e.g. SIFT features are not as
570 precise as least square matches with $\frac{1}{10}$ pixel size accuracies; Grün, 2012) to perform reliable
571 3D reconstruction and thus retrieve an accurate sparse point cloud because optimization
572 procedures for model refinement rely on this first point cloud. Thus, immanent errors will
573 propagate along the different stages of SfM photogrammetry.

574 On the other hand, more obviously image-matching performance is important for dense
575 reconstruction, when 3D information is calculated for almost every pixel. The accuracy of
576 intersection during dense matching depends on the accuracy of the estimated camera
577 orientations (Remondino et al., 2014). If the quality of the DEM is the primary focus, which is
578 usually not the case for SfM algorithms originating from computer vision, the task of image-
579 matching is still difficult (Grün, 2012). Nevertheless, newer approaches are emerging, though,
580 which still need evaluation in respect of accuracy and reliability (Remondino et al., 2014). An
581 internal quality control for image-matching is important for DEM assessment (Grün, 2012),
582 but are mostly absent in tools for SfM photogrammetry.

583 So far, many studies exist, which evaluate the quality of 3D reconstruction in geo-scientific
584 applications. Nevertheless, considerations of dense-matching performance are still missing,
585 especially in regard of rough topographies (Eltner and Schneider, 2015).

586

587 *Surface texture*

588 Texture and contrast of the area of interest is significant to identify suitable homologues
589 image points. Low textured and contrasted surfaces result in a distinct decrease of image
590 features, i.e. snow covered glaciers (Gómez-Gutiérrez et al., 2014) or sandy beaches (Mancini

et al., 2013). Furthermore, vegetation cover complicates image matching performance due to its highly variable appearance from differing viewing angles (e.g. Castillo et al., 2012, Eltner et al., 2015) and possible movements during wind. Thus, in this study, where present, only studies of bare surfaces are reviewed for error assessment.

Illumination condition

Over- and under-exposure of images is another cause of error in the reconstructed point cloud, which cannot be significantly improved by utilising HDR images (Gómez-Gutiérrez et al., 2015). Well illuminated surfaces result in a high number of detected image features, which is demonstrated for coastal boulders under varying light conditions by Gienko and Terry (2014). Furthermore, Gómez-Gutiérrez et al. (2014) highlight the unfavourable influence of shadows because highest errors are measured in these regions; interestingly, these authors calculate the optimal time for image acquisition from the first DEM for multi-temporal data acquisition. Furthermore, the temporal length of image acquisition needs to be considered during sunny conditions because with increasing duration shadow changes can decrease matching performance, i.e. with regard to the intended quality surveys lasting more than 30 minutes should be avoided (Bemis et al., 2014). Generally, overcast but bright days are most suitable for image capture to avoid strong shadows or glared surfaces (James and Robson, 2012).

GCP accuracy and distribution

GCPs are important inputs for data referencing and scaling. Photogrammetry always stresses the weight of good ground control for accurate DEM calculation, especially if one-staged BA is performed. In the common SfM workflow integration of GCPs is less demanding because they are only needed to transform the 3D-model from the arbitrary coordinate system, which is comparable to the photogrammetric two-staged BA processing. A minimum of three GCPs are necessary to account for model rotation, translation and scale. However, GCP redundancy, thus more points, has been shown to be preferable to increase accuracy (James and Robson, 2012). A high number of GCPs further ensures the consideration of checkpoints not included for the referencing, which are used as independent quality measure of the final DEM. More complex 3D reconstruction tools either expand the original 3D-Helmert-transformation by secondary refinement of the estimated interior and exterior camera geometry to account for non-linear errors (e.g. Agisoft PhotoScan) or integrate the ground control into the BA (e.g.

APERO). For instance, Javernick et al. (2014) could reduce the height error to decimetre level by including GCPs in the model refinement.

Natural features over stable areas, which are explicitly identifiable, are an alternative for GCP distributions, although they usually lack strong contrast (as opposed to artificial GCPs) that would allow for automatic identification and sub-pixel accurate measurement (e.g. Eltner et al., 2013). Nevertheless, they can be suitable for multi-temporal change detection applications, where installation of artificial GCPs might not be possible (e.g. glacier surface reconstruction; Piermattei et al., 2015) or necessary as in some cases relative accuracy is preferred over absolute performance (e.g. observation of landslide movements, Turner et al., 2015).

GCP distribution needs to be even and adapted to the terrain resulting in more GCPs in areas with large changes in relief (Harwin and Lucieer, 2012) to cover different terrain types. Harwin and Lucieer (2012) state an optimal GCP distance between $\frac{1}{5}$ and $\frac{1}{10}$ of object distance for UAV applications. Furthermore, the GCPs should be distributed widely across the target area (Smith et al., 2015) and at the edge or outside the study reach (James and Robson, 2012) to enclose the area of interest, because if the study area is extended outside the GCP area, a significant increase of error is observable in that region (Smith et al., 2014, Javernick et al., 2014, Rippin et al., 2015). If data acquisition is performed with parallel-axis UAV images and GCPs are implemented for model refinement, rules for GCP setup according to classical photogrammetry apply, i.e. dense GCP installation around the area of interest and height control points in specific distances as function of image number (more detail in e.g. Kraus, 2007).

The measurement of GCPs can be performed either within the point cloud or the images, preferring the latter because identification of distinct points in 3D point clouds of varying density can be less reliable (James and Robson, 2012, Harwin and Lucieer, 2012) compared to sub-pixel measurement in 2D images, where accuracy of GCP identification basically depends on image quality. Fig. 5 a illustrates that only few studies measured GCPs in point clouds producing higher errors compared to other applications at the same distance.

5.2 Errors due to accuracy/precision assessment technique

Reference of superior accuracy

654 It is difficult to find a suitable reference for error assessment of SfM photogrammetry in geo-
655 scientific or geomorphologic applications due to the usually complex and rough nature of the
656 studied surfaces. So far, either point based or area based measurements are carried out. On the
657 one hand, point based methods (e.g. RTK GPS or total station) ensure superior accuracy but
658 lack sufficient area coverage for precision statements of local deviations; on the other hand,
659 area based (e.g. TLS) estimations are used, which provide enough data density but can lack of
660 sufficient accuracy (Eltner and Schneider, 2015). Roughness is the least constrained error
661 within point clouds (Lague et al., 2013) independent from the observation method. Thus, it is
662 difficult to distinguish between method noises and actual signal of method differences,
663 especially at scales where the reference method reaches its performance limit. For instance
664 Tonkin et al. (2014) indicate that the quality of total station points is not necessarily superior
665 on steep terrain.

666 Generally, 75 % of the investigations reveal a measured error that is 20 times higher than the
667 error of the reference. But the median shows that the superiority of the reference accuracy is
668 actually significantly poorer; the measured error is merely twice the reference error (Fig. 4 c).
669 The reviewed studies further indicate that the superior accuracy of the reference seems to
670 depend on the camera-to-object distance (Fig. 5 b). In shorter distances (below 50 m) most
671 references reveal accuracies that are lower than one magnitude superiority to the measured
672 error. However, alternative reference methods are yet absent. Solely, for applications in
673 further distances the references are sufficient. These findings are relevant for the
674 interpretation of the relative error because low ratios at small scale reaches might be due to
675 the low performance of the reference rather than the actual 3D reconstruction quality but due
676 to the reference noise lower errors are not detectable. Low relative errors are measured where
677 the superior accuracy is also low (distance 5-50 m) and large ratios are given at distance
678 where superior accuracy increases as well.

679

680 *Type of deviation measurement*

681 The reviewed studies use different approaches to measure the distance between the reference
682 and the 3D reconstructed surface. Comparisons are either performed in 2.5D (raster) or real
683 3D (point cloud). Lague et al. (2013) highlight that the application of raster inherits the
684 disadvantage of data interpolation, especially relevant for rough surfaces or complex areas
685 (e.g. undercuts as demonstrated for gullies by Frankl et al., 2015). In this context it is

686 important to note that lower errors are measured for point-to-point distances rather than raster
687 differencing (Smith and Vericat, 2015, Gómez-Guiérrez et al., 2014b).

688 Furthermore, within 3D evaluation different methods for deviation measurement exist. The
689 point-to-point comparison is solely suitable for a preliminary error assessment because this
690 method is prone to outliers and differing point densities. By point cloud interpolation alone
691 (point-to-mesh), this issue is not solvable because there are still problems at very rough
692 surfaces (Lague et al., 2013). Different solutions have been proposed: On the one hand,
693 Abellan et al. (2009) proposed averaging the point cloud difference along the spatial
694 dimension, which can also be extended to 4D (x, y, z, time; Kromer et al., 2015). On the other
695 hand, Lague et al. (2013) proposed the M3C2 algorithm for point cloud comparison that
696 considers the local roughness and further computes the statistical significance of detected
697 changes. Stumpf et al. (2014) and Gómez-Gutiérrez et al. (2015) illustrated lower error
698 measurements with M3C2 compared to point-to-point or point-to-mesh. Furthermore, Kromer
699 et al. (2015) showed how the 4D filtering, when its implementation is feasible, allows to
700 considerably increase the level of detection compared to other well-stablished techniques of
701 comparison.

702

703 ### 5.3 Standardised error assessment

704 To compare the achieved accuracies and precisions of different studies a standardised error
705 assessment is necessary, e.g. considering the theoretical error ratio. The calculation of the
706 theoretical error for the convergent image acquisition schemes is possible, making some basic
707 assumptions about the network geometry, i.e. the strength of image configuration equals 1 (as
708 in James & Robson, 2012), the number of images equals 3 (as in James & Robson, 2012) and
709 an image measurement error of 0.29 due to quantisation noise (as a result of continuous signal
710 conversion to discrete pixel value). However, it is not possible to evaluate the theoretical error
711 for parallel-axes case studies because information about the distance between subsequent
712 images (base) is mostly missing, but essential to solve the equation and should not be
713 assumed. Eltner and Schneider (2015) and Eltner et al. (2015) compare their results to
714 parallel-axes theoretical error and could demonstrate that for soil surface measurement from
715 low flying heights at least photogrammetric accuracy is possible (e.g. sub-cm error for
716 altitudes around 10 m).

717 The results from James and Robson (2012), which show a less reliable performance of SfM
718 than expected from photogrammetric estimation, can be confirmed by the reviewed studies.

719 Image-based 3D reconstruction, considering SfM workflows, performs poorer than the
720 theoretical error (Fig. 5c). The measured error is always higher and on average 90 times worse
721 than the theoretical error. Even for the smallest theoretical error ratio the actual error is 6
722 times higher. Furthermore, it seems that with increasing distance theoretical and measured
723 errors converge slightly.

724 As demonstrated, diverse factors influence SfM photogrammetry performance and subsequent
725 DEM error with different sensitivity. Generally, accurate and extensive data acquisition is
726 necessary to minimise error significantly (Javernick et al., 2014). Independent reference
727 sources, such as TLS, are not replaceable (James and Robson, 2012) due to their differing
728 error properties (i.e. error reliability) compared to image-matching (Grün, 2012). Synergetic
729 effects of SfM and classical photogrammetry should be used, i.e. benefiting from the high
730 automation of SfM to retrieve initial estimates without any prior knowledge about the image
731 scene and acquisition configuration and adjacent reducing error by approved photogrammetric
732 approaches, which are optimised for high accuracies.

733 The reviewed studies indicate the necessity of a standardised protocol for error assessment
734 because the variety of studies inherit a variety of scales worked at, software used, GCP types
735 measured, deviation measures applied, image network configurations implemented, cameras
736 and platforms operated and reference utilised, making it very difficult to compare results with
737 consistency. Relevant parameters for a standard protocol are suggested in Table 5.

738

739 ## 6 Perspectives and limitations

740 SfM photogrammetry has allowed capturing massive three-dimensional datasets by non-
741 specialists during the last five years, and it is highly expected that this technique will evolve
742 during the forthcoming decade. Current studies are focusing on capturing the terrain's
743 geometry with high precision, but several opportunities to improve our understanding,
744 modelling and prediction of different earth surface processes still remain unexplored. For
745 instance, the use of super-macro imagery in conventional SfM workflows is expected to be
746 explored soon for investigating natural phenomena in a much higher level of detail.
747 Nevertheless, some technological issues that need to be addressed include the progressive
748 degradation of the data quality at very short distances due to the effect of a limited depth of
749 field; Up to our knowledge, the use of focus stacking for extending shallow depth of field of
750 single images has not been explored yet. Some other technical and operational aspects are still
751 limiting our ability to derive 3D point clouds from digital imagery over naturally complex

outcrops. Examples include the occurrence of biases and occlusions that can strongly influence the quality of the acquired datasets and the progressive reduction of the ground resolution (meter/pixel) at longer distances, which can be addressed using mobile platforms such as UAV systems. Eventually, SfM photogrammetry technique may become a mainstream procedure in geomorphological studies during the next decade, perspectives include efforts in cross-disciplinarity, process automatisation, data and code sharing, real time data acquisition and processing, unlocking the archives, etc., as follows:

6.1 Cross-disciplinarity

A great potential relies on adapting three dimensional methods originally developed for the treatment of 3D LiDAR data to investigate natural phenomena through SfM photogrammetry techniques. Applications on 3D point cloud treatment dating back from the last decade will soon be integrated into SfM photogrammetry post-processing; Examples include: geomorphological investigations in high mountain areas (Milan et al., 2007), geological mapping (Buckley et al., 2008; Franceschi et al. 2009), soil erosion studies (Eltner and Baumgart, 2015), investigation of fluvial systems (Heritage and Hetherington, 2007, Cavalli et al., 2008; Brasington et al., 2012), and mass wasting phenomena (Lim et al., 2005, Oppikofer et al. 2009, Abellan et al., 2010).

Some other data treatment techniques that have been developed during the last decade and that will be adapted and enriched by the growing SfM photogrammetry community include: automatic lithological segmentation according to the intensity signature (Humair et al., 2015), integration of ground based LiDAR with thermal/hyperspectral imaging for lithological discrimination (Kääb, 2008, Hartzell et al., 2014), extraction of the structural settings on a given outcrop (Jaboyedoff et al., 2007, Sturzenegger and Stead, 2009, Gigli and Casagli, 2011, Riquelme et al., 2014) and the automatic extraction of geological patterns such as surface roughness (Poropat, 2009), discontinuity spacing/persistence/waviness (Fekete et al. 2010, Khoshelham et al., 2011, Pollyea and Fairley, 2011). Concerning 4D data treatment for investigating changes on natural slope, some lessons learned may be adapted from the bi- and three-dimensional tracking of mass movements (Teza et al., 2007, Monserrat and Crosetto 2008), investigation of progressive failures (Royan et al., 2015, Kromer et al., 2015), and from the usage of mobile systems (Lato et al., 2009, Michoud et al., 2015).

6.2 Process-automatisation

785 Handling huge databases is an important issue and although fully automatic techniques may
786 not be necessary in some applications, a series of tedious and manual processes are still
787 required for data treatment.

788

789 ### 6.3 Data and code sharing

790 Open data in geomorphometric studies using point clouds is also needed. The development of
791 open-source software for handling huge 3D datasets such as CloudCompare (Girardeau-
792 Montaut, 2015) has considerably boosted geomorphometric studies using 3D point clouds.
793 Nevertheless, appart from the above mentioned case, sharing the source code or the RAW
794 data of specific applications for investigating earth surface processes is still not well
795 stablished in our discipline. A series of freely available databases exist for LiDAR datasets
796 (openTopography.org, rockbench.com, 3D-landslide.com). But up to the knowledge of these
797 authors, there is no specific Git-Hub cluster or website dedicated to the maintaining and
798 development of open-access software in geosciences.

799

800 ### 6.4 Unlocking the archive

801 The appraisal of digital photography and the exponential increase of data storage capabilities
802 have enabled the massive archive of optical images around the world. Accessing such
803 quantity of information could provide unexpected opportunities for the four dimensional
804 research of geomorphological processes using SfM photogrammetry workflows. Except for
805 some open repositories (e.g. Flickr, Google street view) the possibility to access the massive
806 optical data is still scarce. In addition, accessing to such databases may become a challenging
807 task due to data interchangeability issues. A considerable effort may be necessary for creating
808 such database with homogeneous data formats and descriptors (type of phenomenon, temporal
809 resolution, pixel size, accuracy, distance to object, existence of GCPs, etc.) during the
810 forthcoming years.

811 A first valuable approach to use data from online imagery was presented by Martin-Brualla et
812 al. (2015), who pave the way for further research in a new field of 3D surface analysis (i.e.
813 time-lapse). Other possible applications might unlock the archive of ancient airborne,
814 helicopter-based or terrestrial imaginary, ranging from the estimation of coastal retreat rates,
815 the observation of the evolution of natural hazards to the monitoring of glacier fronts, and
816 further.

817

818 ## 6.5 Real time data acquisition

819 Rapid developments in automatisation (soft- and hardware wise) allow for in situ data
820 acquisition and its immediate transfer to processing and analysing institutions. Thus, extreme
821 events are recognisable during their occurrence and authorities or rescue teams can be
822 informed in real-time. In this context SfM photogrammetry could help to detect and quantify
823 rapid volume changes of e.g. glacier fronts, pro-glacial lakes, rock failures and ephemeral
824 rivers.

825 Furthermore, real-time crowd sourcing offers an entirely new dimension of data acquisition.
826 Due to the high connectivity of the public through smartphones, various possibilities arise to
827 share data (Johnson-Roberson et al., 2015). An already implemented example is real-time
828 traffic information. Jackson and Magro (2015) name further options. Crowd sourced imagery
829 can largely expand possibilities to 3D information.

830

831 ## 6.6 Time-lapse photography

832 A limited frequency of data acquisition increases the likelihood of superimposition and
833 coalescence of geomorphological processes (Abellan et al., 2014). Since time-lapse SfM
834 photogrammetry data acquisition has remained so far unexplored, a great prospect is expected
835 on this topic during the coming years. To date solely James and Robson (2014b) demonstrated
836 its potential by monitoring a lava flow at minute intervals for 37 minutes. One reason why
837 time-lapse SfM photogrammetry remains rather untouched in geosciences lies in the complex
838 nature of producing continuous data sets.

839 Besides the need for an adequate research site (frequent morphodynamic activity), other
840 aspects have to be taken into account: an automatic camera setup is required with self-
841 contained energy supply (either via insolation or wind), adequate storage and appropriate
842 choice of viewing angles onto the area of interest. Furthermore, cameras need to comprise
843 sufficient image overlap and have to be synchronised. Ground control is required and an
844 automatic pipeline for large data treatment should be developed.

845 New algorithms are necessary to deal with massive point cloud databases. Thus, innovative
846 four dimensional approaches have to be developed to take advantage of the information
847 contained in real-time and/or time-lapse monitoring. Combining these datasets with climatic
848 information can improve the modelling of geomorphological processes.

6.7 Automatic UAV surveying

Unmanned airborne vehicles already show a large degree of automatisation as they follow flight paths and acquire data autonomously. Human control is not required except for launching of the multi-copter or fixed wing system. Automatic landing is already provided by several systems. In near future a fully automatic UAV installation could comprise the following: repeated survey of an area of interest, landing and charging at a base station, data link for local storage or satellite based data transfer, and safety mechanism for preventing lift-off during inappropriate weather conditions. However, a large limitation for such realisation lies in legal restrictions because national authorities commonly request for visual contact to the UAV in case of failure. But in remote areas installation of an automatic system could already be allowed by regulation authorities.

6.8 Direct geo-referencing

The use of GCPs is very time-consuming in the current SfM workflow. At first, field efforts are high to install and measure the GCPs during data acquisition. Afterwards, again much time and labour is required during post-processing in order to identify the GCPs in the images, although some progress is made regarding to automatic GCP identification, e.g. by the exploitation of templates (Chen et al., 2000). The efficiency of geo-referencing can be increased significantly applying direct geo-referencing. Thus, the location and position of the camera is measured in real time and synchronised to the image capture by an on-board GPS receiver and IMU (inertial measurement unit) recording camera tilts. This applies to UAV systems as well as terrestrial data acquisition, e.g. by smartphones (Masiero et al., 2014). Exploiting direct geo-referencing can reduce usage of GCPs to a minimum or even replace it, which is already demonstrated by Nolan et al. (2015), who generated DEMs with spatial extents of up to 40 km² and a geo-location accuracy of ± 30 cm.

The technique can be very advantageous when it comes to monitoring areas with great spatial extents or inaccessible research sites. However, further development is necessary, thereby focusing on light-weighted but precise GPS receivers and IMU systems; on UAVs due to their limited payload and for hand-held devices due to their feasibility (e.g. Eling et al., 2015).

7 Conclusions

This review has shown the versatility and flexibility of the recently established method SfM photogrammetry. Due to its beneficial qualities, a wide community of geoscientists starts to implement 3D reconstruction based on images within a variety of studies. Summing up the publications, there are no considerable disadvantages mentioned (e.g. accuracy wise) compared to other methods that cannot be counteracted by placement of GCPs, camera calibration or a high image number. Frontiers in geomorphometry have been expanded once more, as limits of other surveying techniques such as restricted mobility, isolated area of application and high costs are overcome by the SfM photogrammetry. Its major advantages lie in easy-to-handle and cost-efficient digital cameras as well as non-commercial software solutions.

SfM photogrammetry is already becoming an essential tool for digital surface mapping. It is employable in a fully automatic manner but individual adjustments can be conducted to account for each specific case study constrain and accuracy requirement in regard to the intended application. Due to the possibility of different degrees of process interaction, non-experts can utilise the method depending on their discretion.

While research of the last years mainly focussed on testing the applicability of SfM photogrammetry in various geo-scientific applications, recent studies try to pave the way for future usages and develop new tools, setups or algorithms.Performance analysis revealed the suitability of SfM photogrammetry at a large range of scales in regard to case study specific accuracy necessities. However, different factors influencing final DEM quality still need to be addressed. This should be performed under strict experimental (laboratory) designs because complex morphologies, typical in earth surface observations, impede accuracy assessment due to missing superior reference. Thus, independent references and GCPs are still needed in SfM photogrammetry for reliable estimation of the quality of each 3D reconstructed surface.

Fast and straightforward generation of DEMs using freely available tools produces new challenges. The exploitation of the entire information of the SfM photogrammetry output (3D point cloud or mesh instead of 2.5D raster) will become a significant challenge in future studies of high resolution topography (Passalacqua et al., 2015), which has to be even extended to 4D when investigating the evolution along time. Thus, especially comprehensive end user software needs further progress in these aspects.

Appendix A:

Summary of information about reviewed studies used for application evaluation and performance assessment of SfM photogrammetry. Variables are explained in chapter 5.

ID	Author	Year	Application	Software	Perspective	Distance [m]	Scale* [m]	Pixel size [μm]	Image number	Complexity of SfM tool	Measurement error [mm]	Relative error	reference superiority	Theoretical error ratio
1	**Castillo et al.**	**2012**	**gully erosion**	**Bundler + PMVS2**	**terrestrial**	**7**	**7**	**5.2**	**191**	**basic**	**20**	**350**	**-**	**79**
2	**Castillo et al.**	**2014**	**ephemeral gully erosion**	**Bundler + PMVS2**	**terrestrial**	**6**	**25**	**5.2**	**515**	**basic**	**22**	**273**	**11**	**101**
3	**Castillo et al.**	**2015**	**gully erosion**	**SF3M**	**terrestrial**	**10**	**350**	**1.5**	**3095**	**basic**	**69**	**145**	**3.45**	**455**
4	**Dietrich**	**2016**	**riverscape mapping**	**PhotoScan**	**helicopter**	**200**	**10000**	***4.3***	**1483**	**complex**	**730**	**274**	**-**	**-**
5	**Eltner et al.**	**2015**	**soil erosion**	**Pix4D**	**UAV**	**10**	**30**	**2.0, 5.0**	**100**	**complex**	**5, 6**	**2000, 1667**	**-**	**-**
6	**Eltner and Schneider**	**2015**	**soil roughness**	**VisualSfM + PMVS2, PhotoScan, Pix4D, APERO + MicMac, Bundler + PMVS2**	**UAV**	**12**	**15**	**5.0**	**13**	**basic, complex**	**8.1 - 9.8**	**1224 - 1481**	**-**	**-**
7	**Favalli et al.**	**2012**	**geological outcrops, volcanic bomb, stalagmite**	**Bundler + PMVS2**	**terrestrial**	**1**	**0.1 - 0.3**	***5.2***	**30 - 67**	**basic**	**0.3 - 3.8**	**367 - 3333**	**-**	**-**
8	**Fonstad et al.**	**2013**	**bedrock channel and floodplain**	**Photosynth (Bundler implementation)**	**terrestrial**	**40**	**200**	***1.7***	**304**	**basic**	**250**	**160**	**2**	**139**
9	**Frankl et al.**	**2015**	**gully**	**PhotoScan**	**terrestrial**	**2**	**10**	***5.2***	**180 -**	**complex**	**17 - 190**	**11 - 147**	**0 - 4**	**156 - 2184**

			measurement						235					
10	Genchi et al.	2015	bioerosion pattern	VisualSfM + PMVS2	UAV	20	100	*1.5*	400	basic	35	571	-	29
11	Gómez-Gutiérrez et al.	2014	gully headcut	123D Catch	terrestrial	9.3 - 10.5	10	*4.3*	41 - 93	basic	12 - 32	291 - 792	-	31 - 85
12	Gómez-Gutiérrez et al.	2014	rock glacier	123D Catch	terrestrial	300	130	*8.2*	6	basic	430	698	72	103
13	Gómez-Gutiérrez et al.	2015	rock glacier	123D catch, PhotoScan	terrestrial	300	130	*8.2*	9	basic, complex	84 - 1029	-	-	-
14	Immerzeel et al.	2014	dynamic of debris coverd glacial tongue	PhotoScan	UAV	300	3500	*1.3*	284, 307	complex	330	909	-	-
15	James and Robson	2012	volcanic bomb, summit crater, coastal cliff	Bundler + PMVS2	terrestrial, UAV	0.7 - 1000	0.1 - 1600	*5.2, 7.4*	133 - 210	basic	1000 - 2333	0 - 62	1 - 12	16 - 25
16	Javernick et al.	2014	braided river	PhotoScan	helicopter	700	1500	-	147	complex	170	4118	3	-
17	Johnson et al.	2014	alluvial fan, earthquake scarp	PhotoScan	UAV	50, 60	300, 1000	*4.8*	233. 450	complex	130 - 410	122 - 385	-	-
18	Kaiser et al.	2014	gully and rill erosion	PhotoScan	terrestrial	5	10	6.4	-	complex	73 - 141	35 - 68	-	232 - 447
19	Leon et al.	2015	coral reef roughness	PhotoScan	terrestrial (marine)	1.5	250	*1.5*	1370	complex	0.6	2500	-	-
20	Mancini et al.	2013	fore dune	PhotoScan	UAV	40	200	*4.3*	550	complex	110 - 190	211 - 364	4	-
21	Micheletti et al.	2014	river bank, alluvial fan	123D Catch	terrestrial	10, 345	10, 300	*4.8, 1.8*	13	complex	16.8 - 526.3	327 - 595	-	40 - 73
22	Nadal-Romero et al.	2015	badland erosion	PhotoScan	terrestrial	50, 125	50, 100	*5.5*	15, 17	complex	14 - 33	2500 - 4032	1 - 2	6 - 10

23	**Nouwakpo et al.**	**2015**	**microtopography erosion plots**	**PhotoScan**	**terrestrial**	**2**	**6**	***6.4***	**25**	**complex**	**5**	**400**	**-**	**-**
24	**Ouédraogo et al.**	**2014**	**agricultural watershed**	**Apero + MicMac, PhotoScan**	**UAV**	**100**	**200**	***2.0***	**760**	**complex**	**90, 139**	**1111, 719**	**-**	**6, 9**
25	**Piermattei et al.**	**2015**	**debris covered glacier monitoring**	**PhotoScan**	**terrestrial**	**100**	**350**	***4.8, 6.3***	**35, 47**	**complex**	**300, 130**	**333, 769**	**2, 1**	**56, 35**
26	**Prosdocimi et al.**	**2015**	**channel bank erosion**	**PhotoScan**	**terrestrial**	**7**	**30**	***1.4 - 6.3***	**60**	**complex**	**57 - 78**	**90 - 123**	**1**	**143 - 373**
27	**Rippin et al.**	**2015**	**supra-glacial hydrology**	**PhotoScan**	**UAV**	**121**	**2000**	***2.2***	**423**	**complex**	**400**	**303**	**-**	**-**
28	**Ruzic et al.**	**2014**	**coastal cliff**	**Autodesk ReCap**	**terrestrial**	**15**	**50**	***2.0***	**250**	**basic**	**70**	**214**	**1**	**82**
29	**Smith et al.**	**2014**	**post-flash flood evaluation**	**PhotoScan**	**terrestrial**	**50**	**150**	***1.7***	**-**	**complex**	**135**	**370**	**14**	**39**
30	**Smith and Vericat**	**2015**	**badland changes at different scales**	**PhotoScan**	**terrestrial, UAV, AutoGiro**	**5 - 250**	**20 - 1000**	***1.7, 5.5***	**30 - 527**	**complex**	**12.8 - 445**	**132 - 974**	**2 - 89**	**36 - 107**
31	**Snapir et al.**	**2014**	**roughness of soil surface**	**SfMToolkit**	**terrestrial**	**0.6**	**3**	***4.3***	**700**	**basic**	**2.7**	**222**	**270**	**-**
32	**Stumpf et al.**	**2014**	**landslide scarp**	**VisualSfM + CMVS, APERO + MicMac**	**terrestrial**	**50**	**750**	***8.5***	**88 - 401**	**basic, complex**	**27 - 232**	**667 - 1852**	**1 - 3**	**13 - 64**
33	**Tamminga et al.**	**2015**	**change detection after extreme flood event**	**EnsoMOSAIC UAV**	**UAV**	**100**	**200**	***1.3***	**310**	**complex**	**47**	**2128**	**2**	**-**
34	**Tonkin et al.**	**2014**	**moraine-mound topography**	**PhotoScan**	**UAV**	**100**	**500**	***4.3***	**543**	**complex**	**517**	**193**	**-**	**-**
35	**Turner et al.**	**2015**	**landslide change detection**	**PhotoScan**	**UAV**	**40**	**125**	***4.3***	**62 - 415**	**complex**	**31 - 90**	**444 - 1290**	**1 - 3**	**-**
36	**Westoby et al.**	**2012**	**coastal cliff**	**SfMToolkit**	**terrestrial**	**15**	**300**	***4.3***	**889**	**basic**	**500**	**100**	**-**	**-**
37	**Westoby et**	**2014**	**moraine dam,**	**SfMToolkit3**	**terrestrial**	**500**	**500**	***4.3***	**1002,**	**basic**	**814, 85**	**614,**	**2, 43**	**-**

	al.		**alluvial debris fan**						**1054**			**1176**		
38	**Woodget et al.**	**2015**	**fluvial topography**	**PhotoScan**	**UAV**	**26 - 28**	**50, 100**	***2.0***	**32 - 64**	**complex**	**19 - 203**	**138 - 1421**	**-**	**-**
39	**Zarco-Tejada et al.**	**2014**	**tree height estimation**	**Pix4D**	**UAV**	**200**	**1000**	***4.3***	**1409**	**complex**	**350**	**571**	**23**	**-**
40	Bemis et al.	2014	structural geology	PhotoScan	UAV, terrestrial	-	-	-	-	-	-	-	-	-
41	Bendig et al.	2013	crop growth	PhotoScan	UAV	30	7	-	-	-	-	-	-	-
42	Bini et al.	2014	coast erosion/abrasion	Bundler	terrestrial	-	-	-	-	-	-	-	-	-
43	Bretar et al.	2013	(volcanic) surface roughness	APERO + MicMac	terrestrial	1.5	5.9 - 24.6	-	-	-	-	-	-	-
44	Brothelande et al.	2015	post-caldera resurgence	PhotoScan	aircraft	150	6000	*8.2*	7000	-	3100	48	62	-
45	Burns et al.	2015	coral reef	Photoscan	terrestrial (marine)	2	28	-	-	-	-	-	-	-
46	Clapuyt et al.	2015	slope morphology	VisualSFM	UAV	50	100	-	-	-	-	-	-	-
47	Dall'Asta et al.	2015	rock glacier monitoring	APERO + MicMac, Photoscan	UAV	150		-	-	-	-	-	-	-
48	Dandois and Ellis	2013	vegetation mapping	Photoscan	UAV	130	250	-	-	-	-	-	-	-
49	Fernández et al.	2015	landslide	Photoscan	UAV	90	250	-	-	-	-	-	-	-
50	Gienko and Terry	2014	coastal boulders	Photoscan	terrestrial	3	2.5	-	-	-	-	-	-	-
51	Fugazza et al.	2015	glacier mapping	Menci APS	UAV	250	500	-	-	-	-	-	-	-
52	Gomez	2014	volcano morphology	Photoscan	aircraft	-	10000	-	-	-	-	-	-	-
53	Harwin and Lucieer	2012	coastal erosion	Bundler + PMVS2	UAV	120	100	-	1	-	-	-	-	-

54	James and Varley	2012	volcanic dome control	Bundler Photogrammetry package	aircraft	505 – 2420	250	-	-	-	-	-	-	-
55	Kaiser et al.	2015	soil hydraulic roughness	PhotoScan	terrestrial	0.5	1	-	-	-	-	-	-	-
56	Lucieer et al.	2013	landslide	PhotoScan	UAV	40	125	-	-	-	-	-	-	-
57	Lucieer et al.	2014	antartic moss beds	PhotoScan	UAV	50	64	-	-	-	-	-	-	-
58	Meesuk et al.	2014	Urban flooding	VisualSfM	terrestrial	-	-	-	-	-	-	-	-	-
59	Morgenroth and Gomez	2014	tree structure	Photoscan	terrestrial	5	5	-	-	-	-	-	-	-
60	Nouwakpo et al.	2014	soil microtopography	Photoscan	terrestrial	3.1	10	-	-	-	-	-	-	-
61	Stöcker et al.	2015	gully erosion	APERO + MicMac	terrestrial + UAV	2 + 15	35	-	-	-	-	-	-	-
62	Ryan et al.	2015	glacier drainage observation	Photoscan	UAV	500	5000	-	-	-	-	-	-	-
63	Torres-Sánchez et al.	2015	tree plantation	Photoscan	UAV	50, 100	-	-	-	-	-	-	-	-
64	Turner et al.	2015	landslide monitoring	Bundler + PMVS2	UAV	50	-	-	-	-	-	-	-	-
65	Vasuki et al.	2014	structural geology	Bundler + PMVS2	UAV	30 - 40	100	-	-	-	-	-	-	-

These studies are considered for performance analysis.

For most authors not all camera parameters are given. Hence, camera parameters are retrieved from dpreview.com (or similar sources).

* If scale or distance is not given, they are estimated from study area display.

Acknowledgements

The authors A. Eltner, A. Kaiser and F. Neugirg are funded by the German Research Foundation (DFG) (MA 2504/15-1, HA5740/3-1, SCHM1373/8-1). A. Abellan acknowledges support by the Risk Analysis group (Univ. Lausanne) and the UPC (RockRisk research project BIA2013-42582-P).

We would like to thank an anonymous referee and Matt Westoby for their remarks, which significantly improved the manuscript.

References

Abellán, A., Jaboyedoff, M., Oppikofer, T. and Vilaplana, J. M.: Detection of millimetric deformation using a terrestrial laser scanner: experiment and application to a rockfall event, Nat. Hazard Earth Sys., 9, 365–372, 2009.

Abellán, A., Calvet, J., Vilaplana, J. M. and Blanchard, J.: Detection and spatial prediction of rockfalls by means of terrestrial laser scanner monitoring, Geomorphology, 119, 162–171, doi:10.1016/j.geomorph.2010.03.016, 2010.

Abellán, A., Oppikofer, T., Jaboyedoff, M., Rosser, N. J., Lim, M. and Lato, M. J.: Terrestrial laser scanning of rock slope instabilities, Earth Surf. Proc. Landf., 39(1), 80–97. doi:10.1002/esp.3493, 2014.

Ai, M., Hu, Q., Li, J., Wang, M., Yuan, H. and Wang, S.: A Robust Photogrammetric Processing Method of Low-Altitude UAV Images, Remote Sensing, 7, 2302–2333, doi:10.3390/rs70302302, 2015.

Astre, H.: SfMtoolkit. http://www.visual-experiments.com/demos/sfmtoolkit/, last access Nov. 2015.

Bemis, S. P., Micklethwaite, S., Turner, D., James, M. R., Akciz, S., Thiele, S. T. and Bangash, H. A.: Ground-based and UAV-Based photogrammetry: A multi-scale, high-resolution mapping tool for structural geology and paleoseismology, J. Struct. Geol., 69, 163–178, doi:10.1016/j.jsg.2014.10.007, 2014.

Bendig, J., Bolten, A. and Bareth, G.: UAV-based Imaging for Multi-Temporal, very high Resolution Crop Surface Models to monitor Crop Growth Variability, Photogramm. Fernerkun., 6, 551–562, doi:10.1127/1432-8364/2013/02001, 2013.

951 Bini, M., Isola, I., Pappalardo, M., Ribolini, A., Favalli, M., Ragaini, L. and Zanchetta, G.:
952 Abrasive notches along the Atlantic Patagonian coast and their potential use as sea level
953 markers: the case of Puerto Deseado (Santa Cruz, Argentina), Earth Surf. Proc. Landf., 39,
954 1550–1558, doi:10.1002/esp.3612, 2014.

955 Bracken, L. J., Turnbull, L., Wainwright, J. and Bogaart, P.: State of Science Sediment
956 connectivity: a framework for understanding sediment transfer at multiple scales, Earth Surf.
957 Proc. Landf., 40, 177–188, doi:10.1002/esp.3635, 2015.

958 Brasington, J., Vericat, D. and Rychkov, I.: Modeling river bed morphology, roughness, and
959 surface sedimentology using high resolution terrestrial laser scanning, Water Resources
960 Research, 48, W11519, doi:10.1029/2012WR012223, 2012.

961 Bretar, F., Arab-Sedze, M., Champion, J., Pierrot-Deseilligny, M., Heggy, E. and
962 Jacquemoud, S.: An advanced photogrammetric method to measure surface roughness:
963 Application to volcanic terrains in the Piton de la Fournaise, Reunion Island, Remote Sens.
964 Environ., 135, 1–11, doi:10.1016/j.rse.2013.03.026, 2013.

965 Brothelande, E., Lénat, J.-F., Normier, A., Bacri, C., Peltier, A., Paris, R., Kelfoun, K., Merle,
966 O., Finizola, A. And Garaebiti, E.: Insights into the evolution of the Yenkahe resurgent dome
967 (Siwi caldera, Tanna Island, Vanuatu) inferred from aerial high-resolution photogrammetry, J.
968 Volcanol. Geoth. Res., doi:10.1016/j.jvolgeores.2015.04.006, 2015.

969 Brown, M. Z., Burschka, D. and Hager, G. D.: Advances in Computational Stereo, in: IEEE
970 Transactions on pattern analysis and machine intelligence, 25, 993–1008, 2003.

971 Buckley, S., Howell, J., Enge, H. and Kurz, T.: Terrestrial laser scanning in geology: data
972 acquisition, processing and accuracy considerations, J. Geol. Soc. London, 165, 625–638,
973 2008.

974 Burns, J. H. R., Delparte, D., Gates, R. D. and Takabayashi, M.: Integrating structure-from-
975 motion photogrammetry with geospatial software as a novel technique for quantifying 3D
976 ecological characteristics of coral reefs, PeerJ, 3, doi:10.7717/peerj.1077, 2015.

977 Castillo, C., Pérez, R., James, M. R., Quinton, J. N., Taguas, E. V. and Gómez, J. A.:
978 Comparing the Accuracy of Several Field Methods for Measuring Gully Erosion, Soil Sci.
979 Soc. Am. J., 76, doi:10.2136/sssaj2011.0390, 2012.

980 Castillo, C., Taguas, E. V, Zarco-Tejada, P., James, M. R. and Gómez, J. A.: The normalized
981 topographic method: an automated procedure for gully mapping using GIS, Earth Surf. Proc.
982 Landf., 39, 2002–2015, doi:10.1002/esp.3595, 2014.

Castillo, C., James, M. R., Redel-Macías, M. D., Pérez, R. and Gómez, J. A.: SF3M software: 3-D photo-reconstruction for non-expert users and its application to a gully network, SOIL, 1, 583–594, doi:10.5194/soil-1-583-2015, 2015.

Cavalli, M., Tarolli, P., Marchi, L. and Fontana, G. D.: The effectiveness of airborne LiDAR data in the recognition of channel-bed morphology, Catena, 73(3), 249–260, doi:10.1016/j.catena.2007.11.001, 2008.

Chandler, J.: Effective application of automated digital photogrammetry for geomorphological research, Earth Surf. Proc. Landf., 24, 51–63, 1999.

Chen, L. C., Lo, C. Y., Liu, C. L. And Chen, A. J.: Orientation modelling by matching image templates of a GCP database, Proc. 21st ACRS, 21(2), 2000.

Cignoni, P., Callieri, M., Corsini, M., Dellepiane, M., Ganovelli, F. And Ranzuglia, G.: MeshLab: an Open-Source Mesh Processing Tool, in: Eurographics Italian Chapter Conference, Salerno, Italy, 129–136, 2008.

Clapuyt, F., Vanacker, V. and Van Oost, K.: Reproducibility of UAV-based earth topography reconstructions based on Structure-from-Motion algorithms, Geomorphology, doi:10.1016/j.geomorph.2015.05.011, 2015.

Collier, P.: The impact on topographic mapping of developments in land and air survey: 1900-1939, Cartogr. Geogr. Inform., 29(3), 155-174, 2002.

Dall'Asta, E., Delaloye, R., Diotri, F., Forlani, G., Fornari, Morro di Cella, U. M., Pogliotti,P., Roncella, R. and Santise, M.: Use of UAS in a High Mountain Landscape: the Case of Gran Sommetta Rock Glacier (AO). ISPRS – Int. Arch. Photogramm. Rem. Sens., XL-3/W3, 391-397, 2015.

Dandois, J. P. and Ellis, E. C.: High spatial resolution three-dimensional mapping of vegetation spectral dynamics using computer vision, Remote Sens. Environ., 136, 259–276, doi:10.1016/j.rse.2013.04.005, 2013.

Díaz-Varela, R., de la Rosa, R., León, L. and Zarco-Tejada, P.: High-Resolution Airborne UAV Imagery to Assess Olive Tree Crown Parameters Using 3D Photo Reconstruction: Application in Breeding Trials, Remote Sensing, 7, 4213–4232. doi:10.3390/rs70404213, 2015.

1012 Dietrich, J. T.: Riverscape Mapping with Helicopter-Based Structure-From-Motion
1013 Photogrammetry, Geomorphology, 252, 144–157, doi:10.1016/j.geomorph.2015.05.008,
1014 2016.

1015 Ducher, G.: Photogrammetry - The largest operational application of remote sensing,
1016 Photogrammetria, 41(2), 72-82., 1987.

1017 East, A. E., Pess, G. R., Bountry, J. A., Magirl, C. S., Ritchie, A. C., Logan, J. B., Randle, T.
1018 J., Mastin, M. C., Minear, J. T., Duda, J. J., Liermann, M. C., McHenry, M. L., Beechie, T. J.
1019 and Shafroth, P. B.: Reprint of: Large-scale dam removal on the Elwha River, Washington,
1020 USA: River channel and floodplain geomorphic change, Geomorphology, 246, 687–708,
1021 doi:10.1016/j.geomorph.2015.04.027, 2015.

1022 Eling, C., Wieland, M., Hess, C., Klingbeil, L. and Kuhlmann, H.: Development and
1023 evaluation of a UAV based mapping system for remote sensing and surveying applications,
1024 ISPRS – Int. Arch. Photogramm. Rem. Sens., XL-1/W4, 233-239, 2015.

1025 Eltner, A., Mulsow, C. and Maas, H.: Quantitative Measurement of Soil Erosion from Tls and
1026 Uav Data, ISPRS - Int. Arch. Photogramm. Rem. Sens., XL-1/W2, 119–124, 2013.

1027 Eltner, A. and Baumgart, P.: Accuracy constraints of terrestrial Lidar data for soil erosion
1028 measurement: Application to a Mediterranean field plot, Geomorphology, 245, 243–254,
1029 doi:10.1016/j.geomorph.2015.06.008, 2015.

1030 Eltner, A., Baumgart, P., Maas, H.-G. and Faust, D.: Multi-temporal UAV data for automatic
1031 measurement of rill and interrill erosion on loess soil. Earth Surf. Proc. Landf., 40(6), 741–
1032 755, doi:10.1002/esp.3673, 2015.

1033 Eltner, A. and Schneider, D.: Analysis of Different Methods for 3D Reconstruction of Natural
1034 Surfaces from Parallel-Axes UAV Images, Photogramm. Rec., 30(151), 279–299,
1035 doi:10.1111/phor.12115, 2015.

1036 Favalli, M., Fornaciai, A., Isola, I., Tarquini, S. and Nannipieri, L.: Multiview 3D
1037 reconstruction in geosciences, Comput. Geosc., 44, 168–176,
1038 doi:10.1016/j.cageo.2011.09.012, 2012.

1039 Fekete, S., Diederichs, M. and Lato, M.: Geotechnical and operational applications for 3-
1040 dimensional laser scanning in drill and blast tunnels, Tunnelling and Underground Space
1041 Technology, 25(5), 614–628, doi:10.1016/j.tust.2010.04.008, 2010.

1042 Fernández, T., Pérez, J. L., Cardenal, F. J., López, A., Gómez, J. M., Colomo, C., Delgado, J.
1043 and Sánchez, M.: Use of a Light UAV and Photogrammetric Techniques To Study the
1044 Evolution of a Landslide in Jaén (Southern Spain), ISPRS – Int. Arch. Photogramm. Rem.
1045 Sens., XL-3/W3, 241–248, doi:10.5194/isprsarchives-XL-3-W3-241-2015, 2015.

1046 Fonstad, M. A., Dietrich, J. T., Courville, B. C., Jensen, J. L. and Carbonneau, P. E.:
1047 Topographic structure from motion: a new development in photogrammetric measurement,
1048 Earth Surf. Proc. Landf., 38, 421–430, doi:10.1002/esp.3366, 2013.

1049 Frahm, J.-M., Pollefeys, M., Lazebnik, S., Gallup, D., Clipp, B., Raguram, R., Wu, C., Zach,
1050 C. and Johnson, T.: Fast robust large-scale mapping from video and internet photo
1051 collections., ISPRS J. Photogramm., 65(6), 538–549, doi:10.1016/j.isprsjprs.2010.08.009,
1052 2010.

1053 Franceschi, M., Teza, G., Preto, N., Pesci, A., Galgaro, A. and Girardi, S.: Discrimination
1054 between marls and limestones using intensity data from terrestrial laser scanner, ISPRS J.
1055 Photogramm., 64(6), 522–528, doi:10.1016/j.isprsjprs.2009.03.003, 2009.

1056 Francioni, M., Salvini, R., Stead, D., Giovannini, R., Riccucci, S., Vanneschi, C. and Gullì,
1057 D.: An integrated remote sensing-GIS approach for the analysis of an open pit in the Carrara
1058 marble district, Italy: Slope stability assessment through kinematic and numerical methods,
1059 Comp. Geot., 67, 46–63, doi:10.1016/j.compgeo.2015.02.009, 2015.

1060 Frankl, A., Stal, C., Abraha, A., Nyssen, J., Rieke-Zapp, D., De Wulf, A. and Poesen, J.:
1061 Detailed recording of gully morphology in 3D through image-based modelling PhotoScan
1062 Digital Elevation Model (DEM) Soil pipes Structure from M otion–Multi View Stereo
1063 (SfM–MVS) Volume calculation, Catena, 127, 92–101, doi:10.1016/j.catena.2014.12.016,
1064 2014.

1065 Fugazza, D., Senese, A., Azzoni, R. S., Smiraglia, C. Cernuschi, M. Severi, D. D. and
1066 Guglielmina, A.: High-resolution mapping of glacier surface features. The UAV survey of the
1067 Forni glacier (Stelvio National Park, Italy), Geogr. Fis. Dinam. Quat., 38, 25-33,
1068 doi:10.4461/GFDQ.2015.38.03, 2015.

1069 Furukawa, Y., Curless, B., Seitz, S. M. and Szeliski, R.: Towards Internet-scale multi-view
1070 stereo, in: IEEE Conference on Computer Vision and Pattern Recognition, San Francisco,
1071 CA, USA, 1434–1441, doi:10.1109/CVPR.2010.5539802, 2010.

Furukawa, Y. and Ponce, J.: Accurate, dense, and robust multiview stereopsis, in: IEEE Transactions on Pattern Analysis and Machine Intelligence, 83, 1362–1376, doi:10.1109/TPAMI.2009.161, 2010.

Genchi, S. A., Vitale, A. J., Perillo, G. M. E. and Delrieux, C. A.: Structure-from-Motion Approach for Characterization of Bioerosion Patterns Using UAV Imagery, Sensors, 15, 3593–3609, doi:10.3390/s150203593, 2015.

Gienko, G. A. and Terry, J. P.: Three-dimensional modeling of coastal boulders using multi-view image measurements, Earth Surf. Proc. Landf., 39, 853–864, doi:10.1002/esp.3485, 2014.

Gigli, G. and Casagli, N.: Semi-automatic extraction of rock mass structural data from high resolution LIDAR point clouds., Int. J. Rock Mech. Min., 48, 187–198, doi:10.1016/j.ijrmms.2010.11.009, 2011.

Girardeau-Montaut, D.: CloudCompare (version 2.x; GPL software), EDF RandD, Telecom ParisTech, http://www.cloudcompare.org/, last access: Mar. 2015.

Gomez, C.: Digital photogrammetry and GIS-based analysis of the bio-geomorphological evolution of Sakurajima Volcano, diachronic analysis from 1947 to 2006. J. Volcanol. Geoth., 280, 1–13, 2014.

Gomez, C., Hayakawa, Y. and Obanawa, H.: A study of Japanese landscapes using structure from motion derived DSMs and DEMs based on historical aerial photographs: New opportu-nities for vegetation monitoring and diachronic geomorphology, Geomorphology, 242, 11–20, doi:10.1016/j.geomorph.2015.02.021, 2015.

Gómez-Gutiérrez, Á., de Sanjosé-Blasco, J. J., de Matías-Bejarano, J. and Berenguer-Sempere, F.: Comparing Two Photo-Reconstruction Methods to Produce High Density Point Clouds and DEMs in the Corral del Veleta Rock Glacier (Sierra Nevada, Spain), Remote Sensing, 6, 5407–5427, doi:10.3390/rs6065407, 2014.

Gómez-Gutiérrez, Á., Schnabel, S., Berenguer-Sempere, F., Lavado-Contador, F. and Rubio-Delgado, J.: Using 3D photo-reconstruction methods to estimate gully headcut erosion, Catena, 120, 91–101, doi:10.1016/j.catena.2014.04.004, 2014.

Gómez-Gutiérrez, Á., de Sanjosé-Blasco, J., Lozano-Parra, J., Berenguer-Sempere, F. and de Matías-Bejarano, J.: Does HDR Pre-Processing Improve the Accuracy of 3D Models Obtained by Means of two Conventional SfM-MVS Software Packages? The Case of the

1103 Corral del Veleta Rock Glacier, Remote Sensing, 7, 10269–10294, doi:10.3390/rs70810269,
1104 2015.

1105 Gruen, A.: Development and status of image matching in photogrammetry, Photogramm.
1106 Rec., 27(137), 36–57, doi:10.1111/j.1477-9730.2011.00671.x, 2012.

1107 Hartzell, P., Glennie, C., Biber, K., and Khan, S. (2014). Application of multispectral LiDAR
1108 to automated virtual outcrop geology. ISPRS Journal of Photogrammetry and Remote
1109 Sensing, 88, 147–155. doi:10.1016/j.isprsjprs.2013.12.004

1110 Harwin, S. and Lucieer, A.: Assessing the Accuracy of Georeferenced Point Clouds Produced
1111 via Multi-View Stereopsis from Unmanned Aerial Vehicle (UAV) Imagery, Remote Sensing,
1112 4, 1573–1599, doi:10.3390/rs4061573, 2012.

1113 Heritage, G. and Hetherington, D.: Towards a protocol for laser scanning in fluvial
1114 geomorphology, Earth Surf. Proc. Landf., 32(32), 66–74, doi:10.1002/esp.1375, 2007.

1115 Hirschmüller, H.: Semi-Global Matching – Motivation, Developments and Applications,
1116 Photogrammetric Week, 11, 173–184, 2011.

1117 Humair, F., Abellan, A., Carrea, D., Matasci, B., Epard, J.-L. and Jaboyedoff, M.: Geological
1118 layers detection and characterisation using high resolution 3D point clouds: example of a box-
1119 fold in the Swiss Jura Mountains, Eur. J. Rem. Sens., 48, 541–568,
1120 doi:10.5721/EuJRS20154831, 2015.

1121 Immerzeel, W. W., Kraaijenbrink, A., Shea, J. M., Shrestha, A. B., Pellicciotti, F., Bierkens,
1122 M. F. P. and De Jong, S. M.: High-resolution monitoring of Himalayan glacier dynamics
1123 using unmanned aerial vehicles, Rem. Sens. Environ., 150, 93–103,
1124 doi:10.1016/j.rse.2014.04.025, 2014.

1125 Jaboyedoff, M., Metzger, R., Oppikofer, T., Couture, R., Derron, M.-H., Locat, J. and Turmel,
1126 D.: New insight techniques to analyze rock-slope relief using DEM and 3D- imaging cloud
1127 points: COLTOP-3D software. In: Rock Mechanics: Meeting Society's Challenges and
1128 Demands, Eberhardt, E., Stead, D. and Morrison, T. (Eds.), 1st ed., Taylor and Francis,
1129 London, 61–68, 2007.

1130 Jaboyedoff, M., Oppikofer, T., Abellán, A., Derron, M.-H., Loye, A., Metzger, R. and
1131 Pedrazzini, A.: Use of LIDAR in landslide investigations: a review, Nat. Hazards, 61, 5-28,
1132 doi: 10.1007/s11069-010-9634-2, 2012.

1133 Jackson, M. and Magro, G.: Real-time crowd-sourcing, data and modelling. In: IAIA15
1134 Conference Proceedings, Florence, 2015.

1135 James, M. R. and Robson, S.: Straightforward reconstruction of 3D surfaces and topography
1136 with a camera: Accuracy and geoscience application, J. Geoph. Res., 117, F03017,
1137 doi:10.1029/2011JF002289, 2012.

1138 James, M. R. and Varley, N.: Identification of structural controls in an active lava dome with
1139 high resolution DEMs: Volcán de Colima, Mexico, Geoph. Res. Let., 39, L22303,
1140 doi:10.1029/2012GL054245, 2012.

1141 James, M. R. and Robson, S.: Mitigating systematic error in topographic models derived from
1142 UAV and ground-based image networks, Earth Surf. Proc. Landf., 39, 1413–1420,
1143 doi:10.1002/esp.3609, 2014.

1144 James, M. R. and Robson, S.: Sequential digital elevation models of active lava flows from
1145 ground-based stereo time-lapse imagery, ISPRS J. Photogramm. Rem. Sens., 97, 160–170,
1146 doi:10.1016/j.isprsjprs.2014.08.011, 2014.

1147 Javernick, L., Brasington, J. and Caruso, B.: Modeling the topography of shallow braided
1148 rivers using Structure-from-Motion photogrammetry, Geomorphology, 213, 166–182,
1149 doi:10.1016/j.geomorph.2014.01.006, 2014.

1150 Johnson, K., Nissen, E., Saripalli, S., Arrowsmith, J. R., Mcgarey, P., Scharer, K., Williams,
1151 P. and Blisniuk, K.: Rapid mapping of ultrafine fault zone topography with structure from
1152 motion, Geosphere, 10(5), doi:10.1130/GES01017.1, 2014.

1153 Johnson-Roberson, M., Bryson, M., Douillard, B., Pizarro, O. and Williams, S. B.:
1154 Discovering salient regions on 3D photo-textured maps: Crowdsourcing interaction data from
1155 multitouch smartphones and tablets, Comput. Vis. Image Und., 131, 28–41,
1156 doi:10.1016/j.cviu.2014.07.006, 2015.

1157 Kääb, A.: Glacier Volume Changes Using ASTER Satellite Stereo and ICESat GLAS Laser
1158 Altimetry. A Test Study on Edgeøya, Eastern Svalbard, IEEE Transactions on Geoscience
1159 and Remote Sensing, 46(10), 2823 – 2830, doi:10.1109/TGRS.2008.2000627, 2008.

1160 Kääb, A., Girod, L. and Berthling, I.: Surface kinematics of periglacial sorted circles using
1161 structure-from-motion technology, The Cryosphere, 8, 1041–1056, doi:10.5194/tc-8-1041-
1162 2014, 2014.

Kaiser, A., Neugirg, F., Rock, G., Müller, C., Haas, F., Ries, J., and Schmidt, J.: Small-Scale Surface Reconstruction and Volume Calculation of Soil Erosion in Complex Moroccan Gully Morphology Using Structure from Motion, Remote Sensing, 6, 7050–7080, doi:10.3390/rs6087050, 2014.

Kaiser, A., Neugirg, F., Haas, F., Schmidt, J., Becht, M. and Schindewolf, M.: Determination of hydrological roughness by means of close range remote sensing, SOIL, 1, 613–620, doi:10.5194/soil-1-613-2015, 2015.

Khoshelham, K., Altundag, D., Ngan-Tillard, D. and Menenti, M.: Influence of range measurement noise on roughness characterization of rock surfaces using terrestrial laser scanning, Int. J. Rock Mech. Min., 48, 1215–1223, doi:10.1016/j.ijrmms.2011.09.007, 2011.

Kraus, K.: Photogrammetry: Geometry from Images and Laser Scans, 2nd edition, De Gruyter, Berlin, Germany, 459 pages, 2007.

Kromer, R., Abellán, A., Hutchinson, D., Lato, M., Edwards, T. and Jaboyedoff, M.: A 4D Filtering and Calibration Technique for Small-Scale Point Cloud Change Detection with a Terrestrial Laser Scanner, Remote Sensing, 7(10), 13029–13052, doi:10.3390/rs71013029, 2015.

Lague, D., Brodu, N., and Leroux, J.: Accurate 3D comparison of complex topography with terrestrial laser scanner: Application to the Rangitikei canyon (N-Z), ISPRS J. Photogramm. Rem. Sens., 82, 10–26, doi:10.1016/j.isprsjprs.2013.04.009, 2013.

Laussedat, A.: La métrophotographie, Bibliothèque Photographique, Gauthier-Villars, Paris, 55 pages, 1899.

Lato, M., Hutchinson, J., Diederichs, M., Ball, D. and Harrap, R.: Engineering monitoring of rockfall hazards along transportation corridors: using mobile terrestrial LiDAR, Nat. Hazard Earth Sys., 9, 935–946, 2009.

Leon, J. X., Roelfsema, C. M., Saunders, M. I. and Phinn, S. R.: Measuring coral reef terrain roughness using “Structure-from-Motion” close-range photogrammetry, Geomorphology, 242, 21–28, doi:10.1016/j.geomorph.2015.01.030, 2015.

Lim, M., Petley, D. N., Rosser, N. J., Allison, R. J., Long, A. J. and Pybus, D.: Combined digital photogrammetry and time-of-flight laser scanning for monitoring cliff evolution, Photogramm. Rec., 20(110), 109–129, 2008.

1193 Lucieer, A., de Jong, S. and Turner, D.: Mapping landslide displacements using Structure
1194 from Motion (SfM) and image correlation of multi-temporal UAV photography, Prog. Phys.
1195 Geog., 38, 1–20, doi:10.1177/0309133313515293, 2013.

1196 Lucieer, A., Turner, D., King, D. H. and Robinson, S. A.: Using an unmanned aerial vehicle
1197 (UAV) to capture micro-topography of antarctic moss beds, Int. J. Appl. Earth Obs., 27, 53–
1198 62, doi:10.1016/j.jag.2013.05.011, 2014.

1199 Luhmann, T., Robson, S., Kyle, S. and Boehm, J.: Close-Range Photogrammetry and 3D
1200 Imaging, 2nd edition, De Gruyter, Berlin, Germany, 683 pages, 2014.

1201 Mancini, F., Dubbini, M., Gattelli, M., Stecchi, F., Fabbri, S. and Gabbianelli, G.: Using
1202 Unmanned Aerial Vehicles (UAV) for High-Resolution Reconstruction of Topography: The
1203 Structure from Motion Approach on Coastal Environments, Remote Sensing, 5, 6880–6898,
1204 doi:10.3390/rs5126880, 2013.

1205 Martin-Brualla, R., Gallup, D. and Seitz, S. M.: Time-lapse Mining from Internet Photos. in:
1206 IEEE International Conference on Computer Vision (ICCV), 2015.

1207 Masiero, A., Guarnieri, A., Vettore, A. and Pirotti, F.: An ISVD-based Euclidian structure
1208 from motion for smartphones, Int. Arch. Photogramm. Rem. Sens., XL-5, 401-406, 2014.

1209 Meesuk, V., Vojinovic, Z., Mynett, A. E., and Abdullah, A. F.: Urban flood modelling
1210 combining top-view LiDAR data with ground-view SfM observations, Adv. Water Res., 75,
1211 105–117, doi:10.1016/j.advwatres.2014.11.008, 2015.

1212 Micheletti, N., Chandler, J. H. and Lane, S. N.: Investigating the geomorphological potential
1213 of freely available and accessible structure-from-motion photogrammetry using a smartphone,
1214 Earth Surf. Proc. Landf., 40, 473–486, doi:10.1002/esp.3648, 2014.

1215 Micheletti, N., Chandler, J. H. and Lane, S. N.: Structure from Motion (SfM)
1216 Photogrammetry (Chap. 2, Sec. 2.2), In: Cook, S.J., Clarke L.E. and Nield, J.M. (Eds.)
1217 Geomorphological Techniques, British Society of Geomorphology, London, 2015.

1218 Michoud, C., Carrea, D., Costa, S., Derron, M.-H., Jaboyedoff, M., Delacourt, C., Maquaire,
1219 O., Letortu, P. and Davidson, R.: Landslide detection and monitoring capability of boat-based
1220 mobile laser scanning along Dieppe coastal cliffs, Normandy, Landslides, 12(2), 403–418,
1221 2015.

1222 Mikhail, E., Bethel, J. and McGlone, J.: Introduction to Modern Photogrammetry, John Wiley
1223 and Sons, Inc., New York, 479 pages, 2001.

Milan, D. J., Heritage, G. L. and Hetherington, D.: Assessment of erosion and deposition volumes and channel change Application of a 3D laser scanner in the assessment of erosion and deposition volumes and channel change in a proglacial river, Earth Surf. Proc. Landf., 32(32), 1657–1674, doi:10.1002/esp.1592, 2007.

Monserrat, O. and Crosetto, M.: Deformation measurement using terrestrial laser scanning data and least squares 3D surface matching, ISPRS J. Photogramm. Rem. Sens., 63(1), 142–154, doi:10.1016/j.isprsjprs.2007.07.008, 2008.

Morgenroth, J. and Gomez, C.: Assessment of tree structure using a 3D image analysis technique—A proof of concept; Urban Forestry and Urban Greening, 13(1), 198–203, doi:10.1016/j.ufug.2013.10.005, 2014

Nadal-Romero, E., Revuelto, J., Errea, P. and López-Moreno, J. I.: The application of terrestrial laser scanner and SfM photogrammetry in measuring erosion and deposition processes in two opposite slopes in a humid badlands area (central Spanish Pyrenees), SOIL, 1, 561–573, doi:10.5194/soil-1-561-2015, 2015.

Nolan, M., Larsen, C. and Sturm, M.: Mapping snow-depth from manned-aircraft on landscape scales at centimeter resolution using Structure-from-Motion photogrammetry, The Cryosphere Disc., 9, 333–381, doi:10.5194/tcd-9-333-2015, 2015.

Nouwakpo, S. K., James, M. R., Weltz, M. A., Huang, C.-H., Chagas, I. and Lima, L.: Evaluation of structure from motion for soil microtopography measurement, Photogramm. Rec., 29(147), 297–316, doi:10.1111/phor.12072, 2014.

Nouwakpo, S. K., Weltz, M. A. and McGwire, K.: Assessing the performance of Structure-from-Motion photogrammetry and terrestrial lidar for reconstructing soil surface microtopography of naturally vegetated plots, Earth Surf. Proc. Landf., doi:10.1002/esp.3787, 2015.

Oppikofer, T., Jaboyedoff, M., Blikra, L., Derron, M.-H. and Metzger, R.: Characterization and monitoring of the Aknes rockslide using terrestrial laser scanning, Natural Hazards and Earth System Sciences, 9, 1003–1019, 2009.

Ouédraogo, M. M., Degré, A., Debouche, C. and Lisein, J.: The evaluation of unmanned aerial system-based photogrammetry and terrestrial laser scanning to generate DEMs of agricultural watersheds, Geomorphology, 214, 339–355, doi:10.1016/j.geomorph.2014.02.016, 2014.

Passalacqua, P., Belmont, P., Staley, D. M., Simley, J. D., Arrowsmith, J. R., Bode, C. A., Crosby, C., DeLong, S. B., Glenn, N. F., Kelly, S. A., Lague, D., Sangireddy, H., Schaffrath, K., Tarboton, D. G., Wasklewicz, T. and Wheaton, J. M.: Analyzing high resolution topography for advancing the understanding of mass and energy transfer through landscapes: A review. Earth-Sci. Rev., 148, 174–193, doi:10.1016/j.earscirev.2015.05.012, 2015.

Pears, N., Liu, Y. and Bunting, P.: 3D Imaging, Analysis and Applications, Springer, London, 499 pages, 2012.

Piermattei, L., Carturan, L. and Guarnieri, A.: Use of terrestrial photogrammetry based on structure from motion for mass balance estimation of a small glacier in the Italian Alps, Earth Surf. Proc. Landf., 40(13), 1791–1802, doi:10.1002/esp.3756, 2015.

Pierrot-Deseilligny, M. and Clery, I.: APERO, an open source bundle adjustment software for automatic calibration and orientation of set of images, Intern. Arch. Photogramm. Rem. Sens., 38-5(W16), 269–276, 2011.

Pierrot-Deseilligny, M. and Clery, I.: Some possible protocols of acquisition for the optimal use of the "Apero" open source software in automatic orientation and calibration, EuroCow 2012, Barcelona, Spain, (10pp), 2012.

Pike, R. J., Evans, I. S. and Hengl, T.: Geomorphometry: a Brief Guide. In: Hengl, T. and Reuter, H.I. (Eds) Geomorphometry: Concepts, Software, Applications. Developments in Soil Science, 33, 1-28, 2008.

Pollyea, R. and Fairley, J.: Estimating surface roughness of terrestrial laser scan data using orthogonal distance regression, Geology, 39(7), 623–626, doi:10.1130/G32078.1, 2011.

Poropat, G.: Measurement of Surface Roughness of Rock Discontinuities. In Proc. of the 3rd CANUS Rock Mechanics Symposium. Toronto, 2009.

Prosdocimi, M., Calligaro, S., Sofia, G., Dalla Fontana, G. and Tarolli, P.: Bank erosion in agricultural drainage networks: new challenges from Structure-from-Motion photogrammetry for post-event analysis, Earth Surf. Proc. Landf., 40(14), 1891–1906, doi:10.1002/esp.3767, 2015.

Remondino, F., Spera, M. G., Nocerino, E., Menna, F. and Nex, F.: State of the art in high density image matching, Photogramm. Rec., 29(146), 144–166, doi:10.1111/phor.12063, 2014.

Rippin, D. M., Pomfret, A. and King, N.: High resolution mapping of supraglacial drainage pathways reveals link between micro-channel drainage density, surface roughness and surface reflectance, Earth Surf. Proc. Landf., 40(10), 1279–1290, doi:10.1002/esp.3719, 2015.

Royan, M., Abellan, A. and Vilaplana, J.: Progressive failure leading to the 3 December 2013 rockfall at Puigcercós scarp (Catalonia, Spain), Landslides, 12(3), 585–595, 2015.

Ruzic, I., Marovic, I., Benac, C. and Ilic, S.: Coastal cliff geometry derived from structure-from-motion photogrammetry at Stara Baka, Krk Island, Croatia, Geo-Mar. Lett., 34, 555–565, doi:10.1007/s00367-014-0380-4, 2014.

Ryan, J. C., Hubbard, A. L., Box, J. E., Todd, J., Christoffersen, P., Carr, J. R., Holt, T. O., and Snooke, N.: UAV photogrammetry and structure from motion to assess calving dynamics at Store Glacier, a large outlet draining the Greenland ice sheet, The Cryosphere, 9, 1-11, doi:10.5194/tc-9-1-2015, 2015.

Sanz-Ablanedo, E., Rodríguez-Pérez, J. R., Armesto, J. and Taboada, M. F. Á.: Geometric stability and lens decentering in compact digital cameras, Sensors, 10, 1553–1572 doi:10.3390/s100301553, 2010.

Schaffalitzky, F. and Zisserman, A.: Multi-view matching for unordered image sets, or "How do I organize my holiday snaps?", Computer Vision - ECCV 2002, 2350, 414–431. doi:10.1007/3-540-47969-4, 2002.

Shortis, M. R., Bellman, C. J., Robson, S., Johnston, G. J. and Johnson, G. W.: Stability of Zoom and Fixed Lenses used with Digital SLR Cameras, Intern. Arch. Photogramm., Rem. Sens., XXXVI(5), 285–290, 2006.

Siebert, S. and Teizer, J.: Mobile 3D mapping for surveying earthwork projects using an Unmanned Aerial Vehicle (UAV) system, Automation in Construction, 41, 1–14, doi:10.1016/j.autcon.2014.01.004, 2014.

Smith, M. W., Carrivick, J. L., Hooke, J. and Kirkby, M. J.: Reconstructing flash flood magnitudes using "Structure-from-Motion": A rapid assessment tool, J. Hydrol., 519, 1914–1927, doi:10.1016/j.jhydrol.2014.09.078, 2014.

Smith, M. W. and Vericat, D.: From experimental plots to experimental landscapes: topography, erosion and deposition in sub-humid badlands from Structure-from-Motion photogrammetry, Earth Surf. Proc. Landf., 40(12), 1656–1671, doi:10.1002/esp.3747, 2015.

Smith, M. W., Carrivick, J. L. and Quincey, D. J.: Structure from motion photogrammetry in physical geography, Progress in Physical Geography, 1-29, doi: 10.1177/0309133315615805, 2015.

Snapir, B., Hobbs, S. and Waine, T. W.: Roughness measurements over an agricultural soil surface with Structure from Motion, ISPRS J. Photogramm. Rem. Sens., 96, 210–223, doi:10.1016/j.isprsjprs.2014.07.010, 2014.

Snavely, N., Seitz, S. M. and Szeliski, R.: Photo Tourism : Exploring Photo Collections in 3D, ACM Transactions on Graphics, 25(3), 835–846, 2006.

Snavely, N., Seitz, S. M. and Szeliski, R.: Modeling the World from Internet Photo Collections, Intern. J. Comput. Vis., 80(2), 189–210. doi:10.1007/s11263-007-0107-3, 2008.

Stöcker, C., Eltner, A. and Karrasch, P.: Measuring gullies by synergetic application of UAV and close range photogrammetry — A case study from Andalusia, Spain, Catena, 132, 1–11, doi:10.1016/j.catena.2015.04.004, 2015.

Stumpf, A., Malet, J.-P., Allemand, P., Pierrot-Deseilligny, M. and Skupinski, G.: Ground-based multi-view photogrammetry for the monitoring of landslide deformation and erosion, Geomorphology, 231, 130–145, doi:10.1016/j.geomorph.2014.10.039, 2014.

Sturzenegger, M. and Stead, D.: Close-range terrestrial digital photogrammetry and terrestrial laser scanning for discontinuity characterization on rock cuts, Eng. Geol., 106, 163–182, doi:10.1016/j.enggeo.2009.03.004, 2009.

Tamminga, A. D., Eaton, B. C. and Hugenholtz, C. H.: UAS-based remote sensing of Wuvial change following an extreme Wood event, Earth Surf. Proc. Landf., 40(11), 1464–1476, doi:10.1002/esp.3728, 2015.

Thomsen, L., Stolte, J., Baartman, J. and Starkloff, T.: Soil roughness : comparing old and new methods and application in a soil erosion model, SOIL, 1, 399–410, doi:10.5194/soil-1-399-2015, 2015.

Tonkin, T. N., Midgley, N. G., Graham, D. J. and Labadz, J. C.: The potential of small unmanned aircraft systems and structure-from-motion for topographic surveys: A test of emerging integrated approaches at Cwm Idwal, North Wales, Geomorphology, 226, 35–43, doi:10.1016/j.geomorph.2014.07.021, 2014.

Torres-Sánchez, J., López-Granados, F., Serrano, N., Arquero, O. and Peña, J. M.: High-Throughput 3-D Monitoring of Agricultural-Tree Plantations with Unmanned Aerial Vehicle (UAV) Technology, PLOS One, 10(6), doi:10.1371/journal.pone.0130479, 2015.

Triggs, B., McLauchlan, P., Hartley, R. and Fitzgibbon, A.: Bundle Adjustment - A Modern Synthesis. In: Triggs, B., Zisserman, A. and Szeliski, R. (Eds.), Vision Algorithms: Theory and Practice, Springer, Berlin, Germany, LNCS vol. 1883, 298–372, 2000.

Turner, D., Lucieer, A. and de Jong, S.: Time Series Analysis of Landslide Dynamics Using an Unmanned Aerial Vehicle (UAV), Remote Sensing, 7, 1736–1757, doi:10.3390/rs70201736, 2015.

Ullman, S.: The interpretation of structure from motion. Proceedings of the Royal Society B, 203, 405–426, 1979.

Vasuki, Y., Holden, E. J., Kovesi, P. and Micklethwaite, S.: Semi-automatic mapping of geological Structures using UAV-based photogrammetric data: An image analysis approach, Comput. Geosci., 69, 22–32, doi:10.1016/j.cageo.2014.04.012, 2014.

Westoby, M. J., Brasington, J., Glasser, N. F., Hambrey, M. J. and Reynolds, J. M.: "Structure-from-Motion" photogrammetry: A low-cost, effective tool for geoscience applications, Geomorphology, 179, 300–314, doi:10.1016/j.geomorph.2012.08.021, 2012.

Westoby, M. J., Glasser, N. F., Hambrey, M. J., Brasington, J., Reynolds, J. M. and Hassan, M. A. A. M.: Reconstructing historic glacial lakeoutburst floods through numerical modelling and geomorphological assessment: Extreme events in the Himalaya, Earth Surf. Proc. Landf., 39, 1675–1692, doi:10.1002/esp.3617, 2014.

Woodget, A. S., Carbonneau, P. E., Visser, F. and Maddock, I. P.: Quantifying submerged fluvial topography using hyperspatial resolution UAS imagery and structure from motion photogrammetry, Earth Surf. Proc. Landf., 40(1), 47–64, doi:10.1002/esp.3613, 2015.

Wu, C.: Towards linear-time incremental structure from motion, in: International Conference on 3D Vision - 3DV, Seattle, WA, USA, 127–134, 2013.

Wu, C.: Critical configurations for radial distortion self-calibration, in: IEEE Conference on Computer Vision and Pattern Recognition (CVPR), 25 – 32. doi:10.1109/CVPR.2014.11, 2014.

Zarco-Tejada, P. J., Diaz-Varela, R., Angileri, V. and Loudjani, P.: Tree height quantification using very high resolution imagery acquired from an unmanned aerial vehicle (UAV) and

automatic 3D photo-reconstruction methods, Eur. J. Agron., 55, 89–99, doi:10.1016/j.eja.2014.01.004, 2014.

1379 Table 1. Nomenclature and brief definitions of image-based 3D reconstruction related terms

Image-based 3D reconstruction	recording of the three-dimensional shape of an object from overlapping images from different perspectives
Computer Vision	algorithmic efforts to imitate human vision with focus on automation, amongst others, to reconstruct 3D scenes with methods of image processing and image understanding
Structure from Motion (SfM)	fully automatic reconstruction of 3D scenes from 2D images and simultaneous retrieval of the corresponding camera geometry in an arbitrary coordinate system
Photogrammetry	algorithmic efforts to determine 3D model coordinates and camera geometry focussing on accuracy and precise measurement in images
SfM photogrammetry	fully automatic reconstruction of 3D scenes from 2D images and camera geometry with option to set parameters for (photogrammetric) optimisation of accuracy and precision
Dense matching	increase of resolution of point clouds that model 3D scenes by pixel- or patch-wise matching in images of known intrinsic and extrinsic parameters
Stereo matching	reconstruction of object point through matching (in image space, Remondino et al., 2014) between two overlapping images
ulti-View-Stereo (MVS) matching	reconstruction of object point through matching (in object space, Remondino et al., 2014) from multiple overlapping images
Extrinsic parameters	exterior camera geometry comprising position (three shifts) and orientation (three rotations) of the camera projection centre
Intrinsic parameters	interior camera geometry comprising principle distance (distance between projection centre and image sensor), principle point (intersection of perpendicular from projection centre onto image plane) and distortion parameters (e.g. radial distortion)
Bundle adjustment (BA)	least-square optimisation to simultaneously solve for extrinsic (and intrinsic) parameters of all images; the term bundle correlates to rays that derive from 3D points, converge in corresponding projection centres and intersect with image sensor
Camera self-calibration	intrinsic camera parameters are included as additional unknowns into BA to solve for interior camera geometry
Ground Control Point (GCP)	in images clearly distinguishable point whose object coordinates are known to geo-reference surface model
Digital Elevation Model (DEM)	3D description of the surface in either raster (grid) or vector (mesh) format
Point cloud	quantity of points of 3D coordinates describing the surface within arbitrary or geo-referenced coordinate system, additional information such as normals or colours possible

1380

1381 Table 2: Summary of non-commercial software tools beneficial for SfM photogrammetry processing and post-processing.

Software		*Bundler*	*PMVS2*	*Apero+ MicMac*	*SfMToolkit*	*Meshlab*	*Cloud Compare*	*Sfm_georef*	*VisualSFM*	*SF3M*	*Photosynth*	*123D Catch*
Type		Open Source	Open Source	Open Source	Open Source	Open Source	Open Source	Freely-available	Freely-available	Freely-available	Free web service	Free web service
Website		http://www.cs.cornell.edu/~snavely/bundler	http://www.di.ens.fr/pmvs	http://logiciels.ign.fr/?Micmac	http://www.visual-experiments.com/demos/sfmtoolkit	http://meshlab.sourceforge.net	http://www.danielgm.net/cc	http://www.lancaster.ac.uk/staff/jamesm/software/sfm_georef.htm	http://ccwu.me/vsfm	http://sf3map.csic.es	https://photosynth.net	http://www.123dapp.com/catch
Operative system		Linux Windows	Linux Windows	Linux Mac Windows	Windows	Mac Windows	Linux Mac Windows	Windows	Linux Mac Windows	Windows	Windows	Windows Mac
Functionalities	*Camera calibration*			x								
	Bundle adjustment	x			x				x	x	x	x
	Bundle adjustment with GCPs			x								
	Sparse 3D re-construction	x		x	x				x	x	x	x
	Geo-referencing			x				x	x	x		
	Dense 3D re-construction		x	x					x	x		x
	Post-processing			x						x		
	Advanced cloud processing					x	x					

1382 Table 3: Key developments of SfM photogrammetry towards a standard tool in
1383 geomorphometry

1384
1385

key developments	authors
method introduction	James & Robson (2012), Westoby et al. (2012), Fonstad et al. (2013)
evaluation of accuracy potential	James & Robson (2012), Westoby et al. (2012), Castillo et al. (2012)
SfM with terrestrial images	James & Robson (2012), Westoby et al. (2012), Castillo et al. (2012)
SfM with UAV images	Harwin & Lucieer (2012)
application with mm resolution	Bretar et al. (2013), Snapir et al. (2014)
application covering km²	Immerzeel et al. (2014)
mitigation of systematic errors (i.e. dome)	James & Robson (2014a), Eltner & Schneider (2015)
influence of image network geometry	Stumpf et al. (2014), Micheletti et al. (2014), Piermattei et al. (2015)
usage of Smartphone for data acquisition	Micheletti et al. (2014)
time-lapse implementation	James & Robson (2014b)
influence of scale	Smith & Vericat (2015)
comparing tools and cameras	Eltner & Schneider (2015)
synergetic usage of terrestrial and aerial images	Stöcker et al. (2015)
sub-merged topography	Woodget et al. (2015)
under water application	Leon et al. (2015)
reuse of historical images	Gomez et al. (2015)

1386

Table 4. Overview of the publication history divided in the main topics from 2012 until editorial deadline in Nov. 2015. Several publications examined more than one topic resulting in a larger number of topics than actual publications (number in brackets in last row). IDs refer to the table in appendix A1.

Topic	2012	2013	2014	2015	2016	ID	Total number of publications on the respective topic
Soil science/erosion	1	-	5	9	-	1, 2, 3, 5, 6, 9, 11, 18, 22, 23, 30, 31, 55, 60, 61	15
Volcanology	3	1	1	1	-	7, 15, 43, 44, 52, 54	6
Glaciology	-	-	4	6	-	12, 13, 14, 25, 27, 34, 37, 47, 51, 62	10
Mass movements	-	1	1	3	-	32, 35, 49, 56, 64	5
Fluvial morphology	-	1	5	3	1	4, 8, 16, 17, 21, 26, 29, 33, 37, 38	10
Coastal morphology	3	1	3	-	-	15, 20, 28, 36, 42, 50, 53	7
Others	1	2	8	5	-	7, 10, 17, 19, 24, 39, 40, 41, 45, 46, 48, 57, 58, 59, 63, 65	16
Topics (publications)	8 (6)	6 (6)	27 (25)	27 (27)	1(1)		69 (65)

1396 Table 5: Data acquisition and error assessment protocol for SfM photogrammetry;
1397 independent from individual study design.

in the field:					
target specifics	study area extent		**ground control specifics**	GCP measurement (total station, GPS, …)	
	sensor to surface distance			GCP description	
	ground sampling distance			GCP number	
	target complexity			GCP accuracy	
camera specifics	camera name		**image acquisition specifics**	illumination condition	
	camera type (SLR, CSC, …)			image number	
	lens type (zoom - fixed)			image overlap	
	sensor resolution			base (distance between images)	
	sensor size			network configuration (conv. - parallel-axis)	
	pixel size			perspective (aerial - terrestrial)	
	focal length		notes		
at the office:					
data processing specifics	SfM tool		**accuracy assessment**	registration residual	
	GCP integration (1-/2-staged)			reference type (LiDAR, RTK pts, …)	
	output data type			reference error	
error ratios	relative error			error measure (M3C2, raster difference, …)	
	reference superiority			statistical value (RMSE, std dev, …)	
	theoretical error ratio		notes		

1398

1399 Figure captions

1400

1401 Figure 1: Schematic illustration of the versatility of SfM photogrammetry.

1402

1403 Figure 2. Map of the research sites of all studies of this review.

1404

1405 Figure 3. Variety of SfM photogrammetry tools used in the 65 reviewed studies.

1406

1407 Figure 4. Boxplots summarizing statistics: a) of the scale of the study reaches (N: 56; ID 1-3
1408 and 5-39 in Appendix A), b) the relative error (calculated in regard to distance and measured
1409 error, N: 54; ID 1-3, 5-12 and 14-39 in Appendix A), and c) the reference superiority
1410 (calculated in regard to measured error and reference error, N: 33; ID 1-30 and 32-39 in
1411 Appendix A) of reviewed studies.

1412

1413 Figure 5. Performance of several error parameters in regard to the camera to surface
1414 distance.a) Characteristics of measured error and relative error (N: 54; ID 1-3, 5-12 and 14-39
1415 in Appendix A) . For grey coloured points GCPs are measured in point cloud (in total 9 times
1416 corresponding to the studies: ID 8, 11, 12, 28, 36, 37 in Appendix A) and for white points
1417 GCPs are measured in images (corresponding to the remaining studies) for model
1418 transformation. b) Superiority of the reference data (N: 33), which is calculated as ratio
1419 between measured error and error of the reference. Area based (ID 5-7, 12, 15, 17, 22, 25, 26,
1420 30 and 32 in Appendix A) and point based (ID 2, 3, 8, 9, 20, 24, 28-30, 33, 35 and 37 in
1421 Appendix A) reference measurements are distinguished. c) Theoretical error ratio, considering
1422 the theoretical and measured error, to illustrate SfM photogrammetry performance in field
1423 applications (N: 23; ID 1-3, 8, 10-12, 15, 21, 22, 25, 26, 28-30 and 32 in Appendix A).
1424

1425

1426 Figure 1:

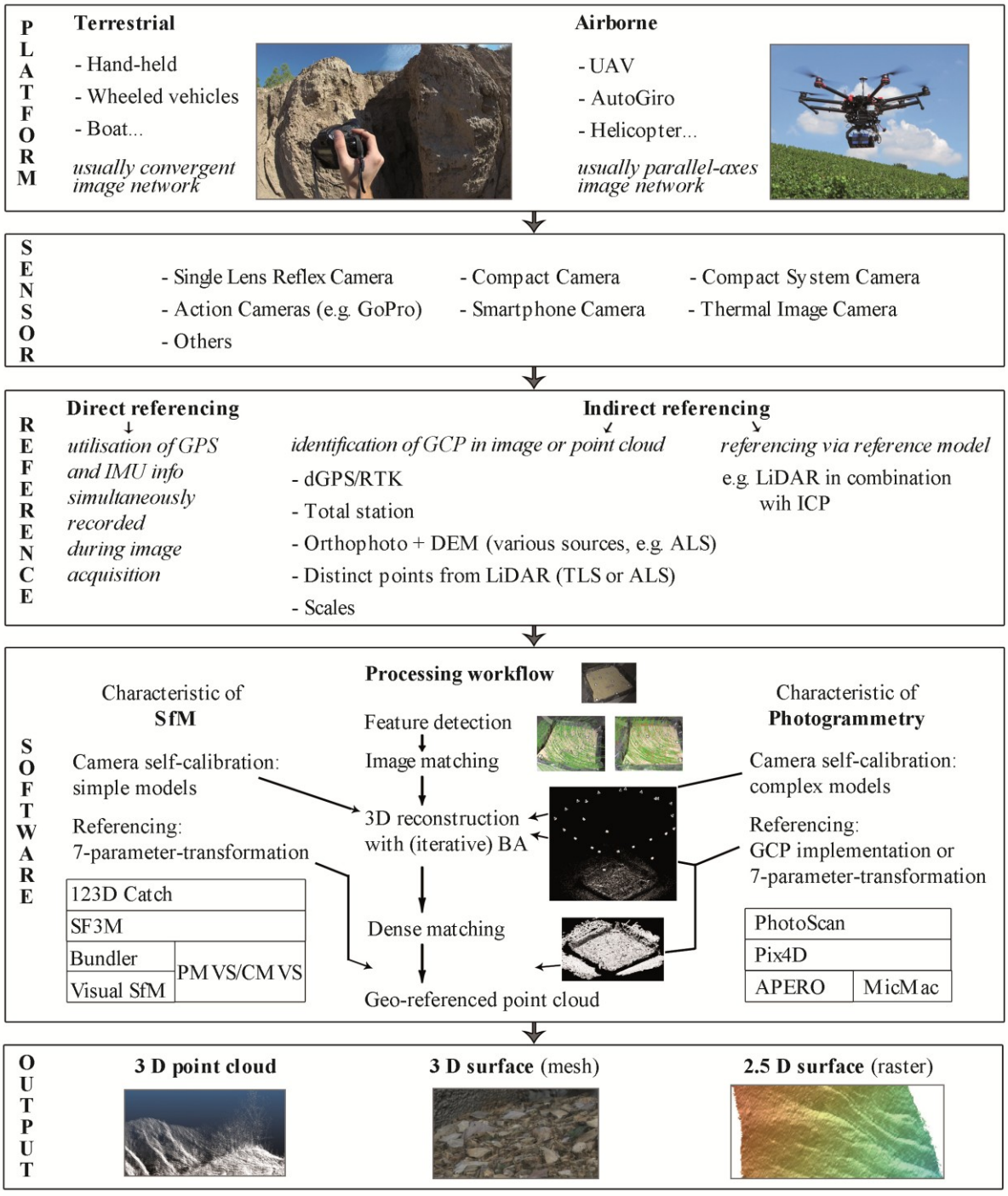

1427

1428

Figure 2:

1432 Figure 3:

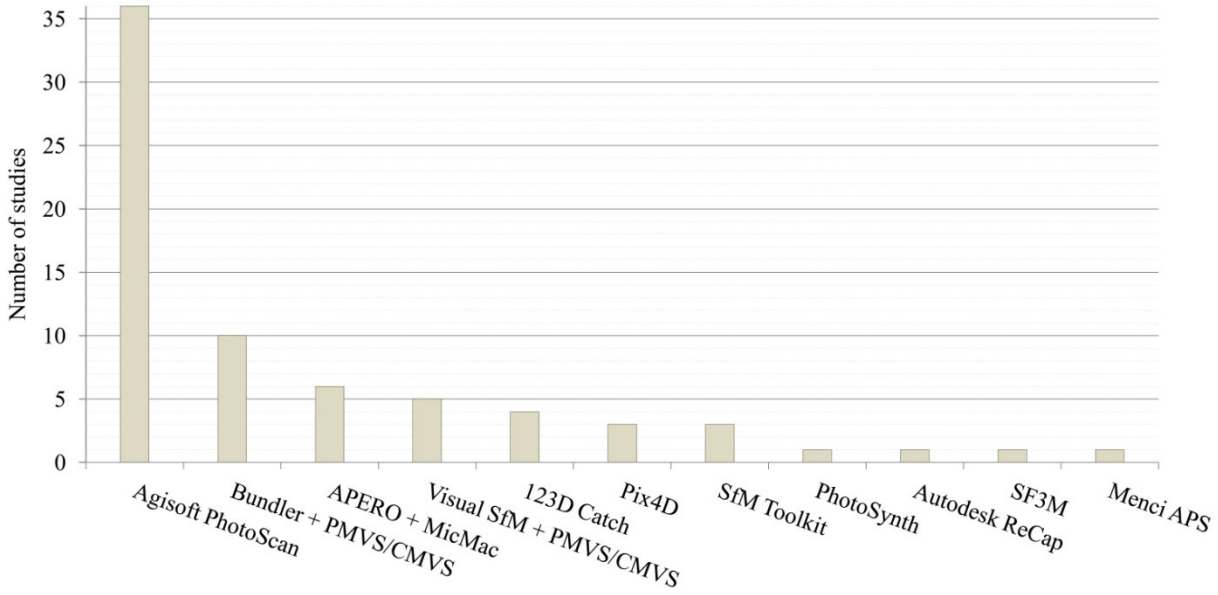

1433

1434

1435 Figure 4:

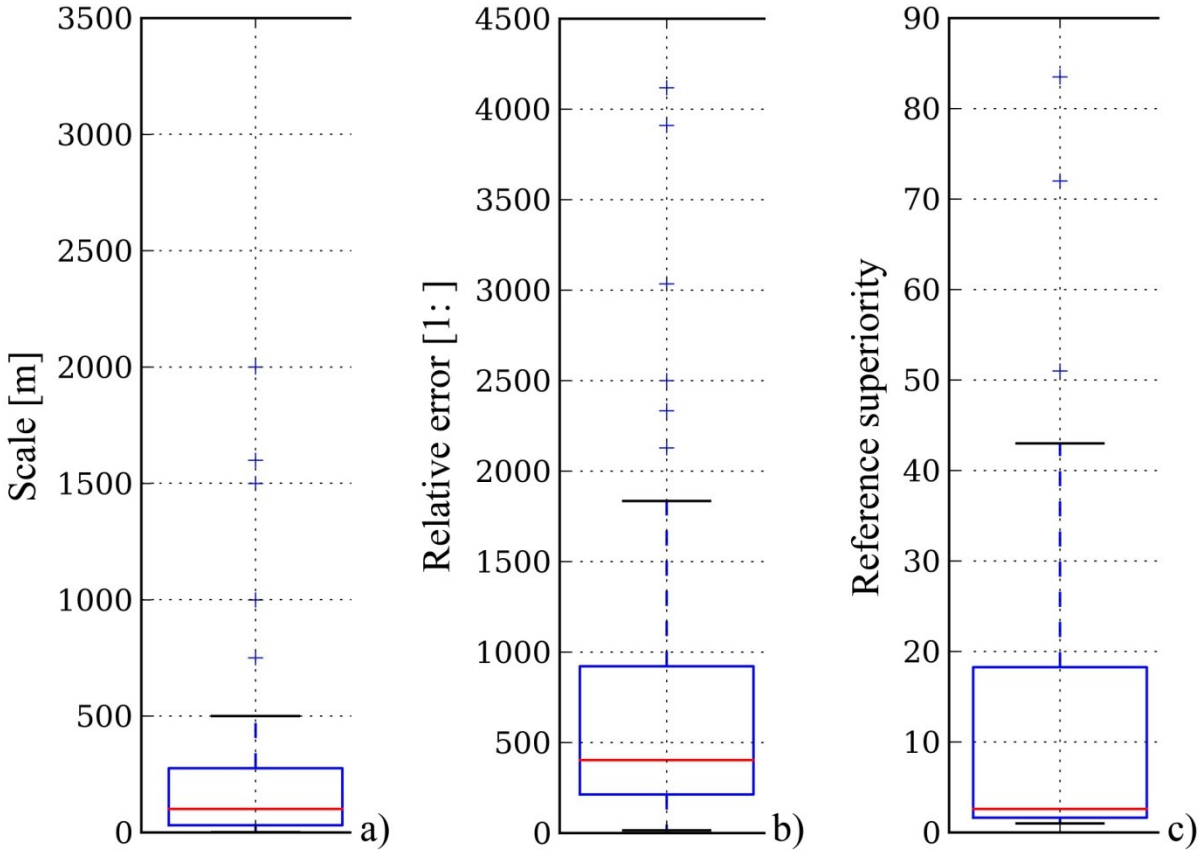

1436

1437

1438 Figure 5:

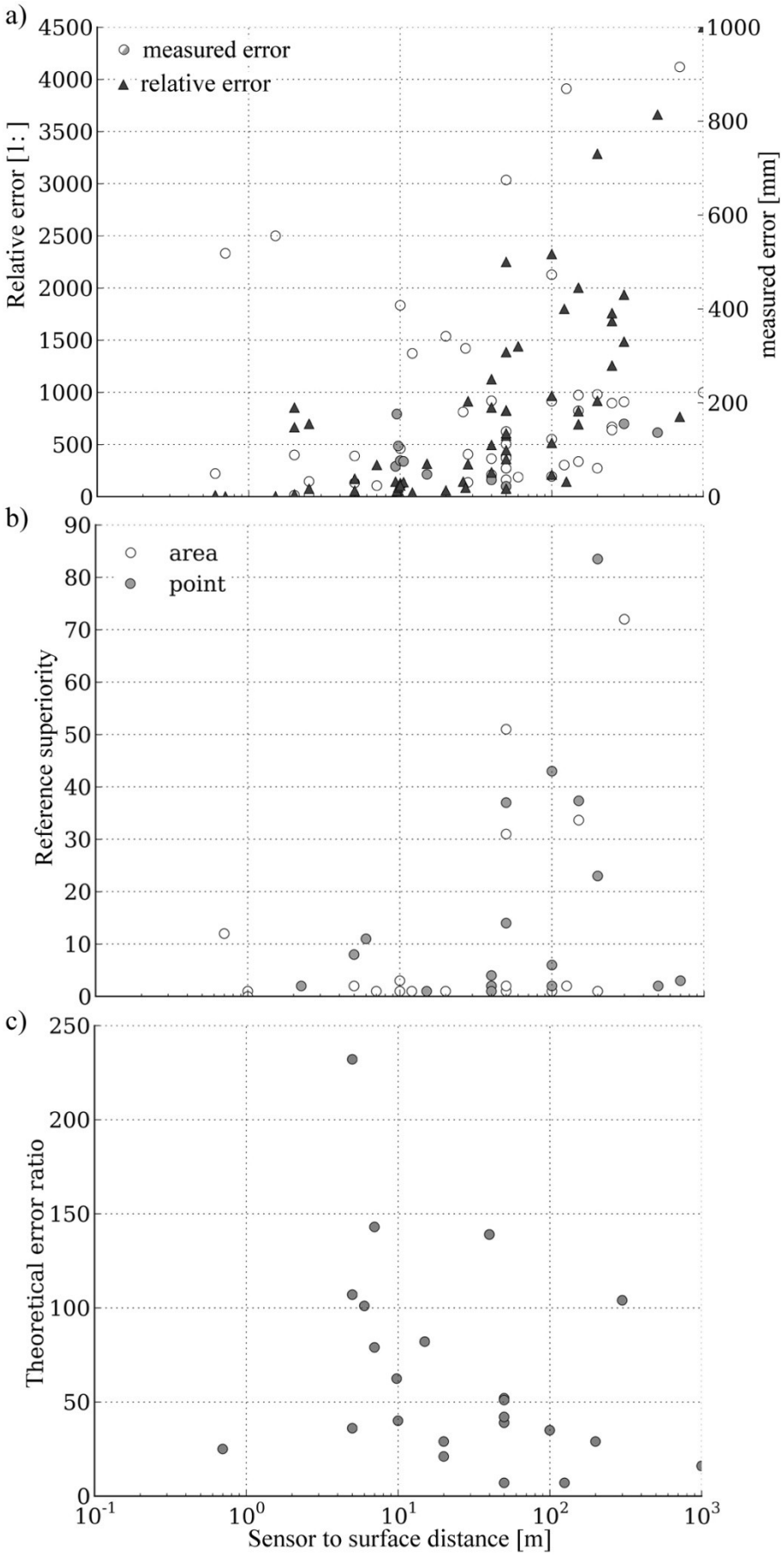

1439